DISTURBING EARTH'S PROTECTIVE SHIELD: PROPAGATION OF MAGNETOSHEATH JETS AND THEIR EFFECTS ON THE MAGNETOPAUSE

EVA KRÄMER

Doctoral Thesis

Main supervisor:
MARIA HAMRIN

Assistant supervisor:
HERBERT GUNELL
TIMO PITKÄNEN
SHAHAB FATEMI

Opponent:
KATARIINA NYKYRI

Examination committee:
ANDRIS VAIVADS
EMILIYA YORDANOVA
CAROL NORBERG

Department of Physics
Faculty of Science and Technology
Umeå University
Umeå, Sweden

September 2026

UMEÅ UNIVERSITET

Eva Krämer: *Disturbing Earth's protective shield:*
Propagation of Magnetosheath Jets and Their Effects on the Magnetopause
© September 2026

ISBN: 978-91-6850-027-0 (print)
ISBN: 978-91-6850-028-7 (pdf)

Printed by: Scandinavian Print Group, Skarpnäck 2026

Umeå, Sweden, 2026

ABSTRACT

SAMMANFATTNING

LIST OF APPENDED PAPERS

PAPER I

Krämer, E., Hamrin, M., Gunell, H., Karlsson, T., Steinvall, K., Goncharov, O., & André, M. (2023). *Waves in magnetosheath jets—classification and the search for generation mechanisms using MMS burst mode data*. Journal of Geophysical Research: Space Physics, 128(7).
https://doi.org/10.1029/2023JA031621

PAPER II

Krämer, E., Fatemi, S., Hamrin, M., Gunell, H., & Semrén, G. (2025). *On the kinetic energy input of magnetosheath jets into the magnetosheath*. Geophysical Research Letters, 52(15).
https://doi.org/10.1029/2025GL115260

PAPER III

E. Krämer, S. Fatemi, M. Hamrin, A. Pöppelwerth, H. Gunell & N. Grimmich (manuscript), *Magnetosheath Jet Interaction with the Magnetopause: Results from the 3D hybrid-kinetic Simulation Amitis*.

PAPER IV

Krämer, E., Hamrin, M., Gunell, H., Baddeley, L., Partamies, N., Raptis, S., ... & Schillings, A. (2025). *Magnetosheath jet-triggered ULF waves: Energy deposition in the ionosphere*. Journal of Geophysical Research: Space Physics, 130(4).
https://doi.org/10.1029/2025JA033792

PAPER V

Mohammed-Amin, T., **Krämer, E.**, Nesbit-Östman, S., Gunell, H., Wedlund, C. S. (2025). *Jets downstream of the Martian bow shock – Occurrence in the 2014–2024 period*. Astronomy & Astrophysics: Planets and planetary systems, 696, A75.
https://doi.org/10.1051/0004-6361/202453557

PAPER VI

Albers, R., Andrews, H., Boccacci, G., Pires, V. D., Laddha, S., Lundén, V., Maraqten, N., Matias, J., **Krämer, E.**, ... & Knutsen, E. W. (2024). *Magnetospheric Venus Space Explorers (MVSE) mission: A proposal for understanding the dynamics of induced magnetospheres*. Acta Astronautica, 221, 194-205.
https://doi.org/10.1016/j.actaastro.2024.05.017

LIST OF RELATED PAPERS

Semrén, G., Hamrin, M., **Krämer, E.**, Dredger, P., Fatemi, S., Lopez, R.E., Milan, S.E., Pitkänen, T., Karlsson, T., Goncharov, O. (2025). Statistical Observations in Support of Bow Shock Current Closure to Earth's High-Latitude Ionosphere During Non-Zero IMF By. *Journal of Geophysical Research: Space Physics*
https://doi.org/10.1029/2024JA033599

Raptis, S., Lindberg, M., Liu, T. Z., Turner, D. L., Lalti, A., Zhou, Y., and Kajdič, P., Kouloumvakos, A., Sibeck, D. G., Vuorinen, L., Michael, A., Shumko, M., Osmane, A., **Krämer, E.,** Turc, L., Karlsson, T., Katsavrias, C., Wilson III, L. B., Madanian, H., Blanco-Cano, X., Cohen, I. J., Escoubet, C. P. (2025). Multimission observations of relativistic electrons and high-speed jets linked to shock-generated transients. *The Astrophysical Journal Letters*
https://doi.org/10.3847/2041-8213/adb154

Fatemi, S., Hamrin, M., **Krämer, E.**, Gunell, H., Nordin, G., Karlsson, T., Goncharov, O. (2024). Unveiling the 3D structure of magnetosheath jets. *Monthly Notices of the Royal Astronomical Society*
https://doi.org/10.1093/mnras/stae1456

Gunell, H., Hamrin, M., Nesbit-Östman, S., **Krämer, E.** (2023). Magnetosheath jets at Mars. *Science Advances*, 9(22).
https://doi.org/10.1126/sciadv.adg57034

Hamrin, M., Schillings, A., Opgenoorth, H., Nesbit-Östman, S., **Krämer, E.**, Araújo, J., Baddeley, L., Gunell, H., Pitkänen, T., Gjerloev, J., Barnes R. J. (2023). Space weather disturbances in non-stormy times: Occurrence of dB/dt spikes during three solar cycles. *Journal of Geophysical Research: Space Physics*
https://doi.org/10.1029/2023JA031804

Pitkänen, T., Chong, G. S., Hamrin, M., Kullen, A., Vanhamäki, H., Park, J.-S., Nowada, M., Schillings, A. **Krämer, E.** Fast Earthward Convection in the Magnetotail and Nonzero IMF By: MMS Statistics. (2023) *Journal of Geophysical Research: Space Physics*
https://doi.org/10.1029/2023JA031593

ACKNOWLEDGMENTS

This part of the thesis was one of the most difficult to write—not because I am not grateful for all the support I have received, but because it is difficult to put that gratitude into words. But, I will give it a try.

First of all, I would like to thank my main supervisor, Maria Hamrin, for introducing me to space plasma physics during my undergraduate studies and for ultimately having faith in me as your PhD student. Thank you for all your encouraging words, guidance, and support, regardless of the direction my research took or where in the world I happened to be.

Secondly, I would like to thank my co-supervisors, Herbert Gunell, Shahab Fatemi, and Timo Pitkänen, for all your support over the years. This thesis would look very different without your scientific input. Herbert, thank you for always taking the time to engage in scientific discussions and for patiently answering my endless questions. Thank you also for your Rhino drawings, it is a bit like the acknowledgements section of a thesis, the part I always looked for first when receiving feedback on a paper from you. Shahab, thank you for introducing me to the world of simulations and for continuously challenging my research.

Thank you to all the past and present Space Girls and Boys—Anja, Audrey, Arnaud, Danny, Gabriella, Jakub, Jeremias, Juan Carlos, Julia, Katerina, Lena, and Siung—for the many scientific and non-scientific discussions during fikas, lunches, and beers. A special thanks to Audrey, Siung, Joan, and Sara for the various skiing activities, IKSU classes, and pancakes at Grössjön. Thank you, Anja, for joining me on Friday swims, going on topptur, and introducing me to the world of pour-over coffee. Thank you, Gabriella, we might not share many interests outside of work, but thank you for being a good friend. Fritz, thank you for the chats in your office and the potlucks. I would also like to thank all my colleagues at the Department of Physics with whom I shared lunches, fikas, and activities outside of work.

A heartfelt thank you to the space physics group at UNIS for welcoming me and introducing me to the world of ionospheric research. Lotte, in particular, thank you for all the tea, for taking me hiking, and for being my polar bear guard. I would also like to thank the Division for Integrated Studies at the Institute for Space-Earth Environmental Research, Nagoya University, for welcoming me and introducing me to radiation belt physics as well as a wide range of Japanese foods. In addition, I had the opportunity to work with the magnetosheath jet community. A special thanks to the members of the jet journal club—Adrian L., Adrian P., Florian, Georg, Jonas, Laura, Luis, Niki, Savvas, and Tara—for the incredibly helpful scientific discussions

and for collaborating on a review paper. I would also like to thank the members of Team Yellow at the Alpbach Summer School for working together on a mission proposal that would even allow us to observe jets at Venus.

Thank you for all the guides at IKSU frilufts for welcoming me into the community and sharing various outdoor activities.

Finally, I would like to thank my family for their unconditional support. My parents, Katrin and Michael, thank you for supporting me in my life choices—even when that meant moving 2000 km away from home—and for still visiting Umeå every year despite the lack of good baguettes, croissants, cheese, and wine. Katrin, thank you for sending endless supplies of Getreidekaffee to wherever I am in the world. Michael, thank you for all the discussions about how to become a better programmer. My brother, Johannes, thank you for all the adventures over the years, and for proving that you are, in fact, a much cooler person than I thought when we were growing up together. To Gun and Daniel, thank you for welcoming me into the Zakrisson family and into Hälsingfors—my second home and a wonderful place for woodworking and gardening. Lastly, Johan, thank you for your love, your support, making me laugh, and for being my partner in crime in exploring many new hobbies.

CREDITS

This work was supported by Vetenskapsrådet grant 2018-03623 and the Swedish National Space Agency under grant 2022-00138.

We also acknowledge the EuroHPC Joint Undertaking for providing computational resources for this project through access to the EuroHPC VEGA, hosted by IZUM/Slovenia, through project EHPC-REG-2023R03-023, granted to Shahab Fatemi.

CONTENTS

1 INTRODUCTION

Space is not empty, in fact, it is filled with a state of matter called *plasma*. Plasma is sometimes referred to as the fourth state of matter and consists of charged particles, positively charged ions and negatively charged electrons. In a plasma, the motion of these charged particles is dominated by the collective behavior due to electromagnetic forces rather than the movement of individual particles.

While on Earth most matter is either solid, liquid, or in gas form, plasma is in fact the most abundant state of the observable matter in our Universe. Stars, like the Sun, are made of plasma and the space in between galaxies and stars is also filled with plasma. Thus, plasma processes control the behavior of most observable matter in the Universe, making their understanding essential for describing astrophysical and space environments. Although we can create plasmas in laboratories, it is difficult to confine the plasma and reproduces the time and spatial scales found in space. As a result, space[1] is a unique natural laboratory for studying plasma processes under conditions that cannot be replicated on Earth. Specifically, we can send up spacecraft that carry scientific instruments to probe plasma processes in our solar system. By learning about the plasma processes in our solar system, we also gain better understanding on plasma processes work outside of the solar system since plasma processes are universal.

In our solar system, the Sun is a major plasma source, by emitting the *solar wind*. The solar wind consists mostly of protons and electrons and fills our entire solar system. The solar wind also carries the Sun's magnetic field with it which makes up the *Interplanetary Magnetic Field*. In addition to the solar wind, solar radiation ionizes the upper layers of planetary atmospheres, creating regions of plasma such as Earth's *ionosphere*.

As the solar wind expands outward in the solar system, planets act as an obstacle to the solar wind. In the case of Earth, the primary obstacle is not the atmosphere itself but the Earth's intrinsic magnetic field. This magnetic field forms a protective cavity known as the *magnetosphere*. Because the solar wind typically flows faster than information can propagate through it (it is *supermagnetosonic*), it cannot adjust smoothly to the presence of this obstacle. Instead, a shock wave forms upstream of Earth, known as the *bow shock*. At this boundary, the solar wind plasma is abruptly decelerated, compressed, and heated.

Downstream of the bow shock lies the *magnetosheath*, a region filled with shocked solar wind plasma. This region is characterized by strong

1 Plasma can be found from about 80 km altitude.

fluctuations in plasma properties and is the primary focus of this thesis. As the plasma flows through the magnetosheath, it is deflected around the magnetosphere. The outer boundary of the magnetosphere is called the *magnetopause*, which separates Earth's magnetic environment from the surrounding solar wind plasma. This boundary plays a crucial role in regulating the transfer of energy and momentum into the magnetosphere.

Why is this important? Although the magnetosphere acts as a protective cavity, it is not impenetrable. Energy and particles from the solar wind can still enter and drive the near-Earth environment, for example, northern lights are created by this interaction[2]. The extent of this interaction depends on the properties of the solar wind, which are highly variable. Changes in solar wind speed, density, and magnetic field can significantly alter how much energy is transferred into the magnetosphere over time.

The solar wind properties and their effects on the planetary environment are a part of what is known as *space weather*. Space weather effects include auroral display but under more extreme conditions also disturbances in radio communication, and induced currents in electric power lines. While certain, extreme solar wind properties are the most prominent drives of space weather, smaller-scale and more localized structures can also play an important role.

One such structure is *magnetosheath jets*. These are transient, localized enhancements in plasma flow and/or the plasma density such that the pressure is locally enhanced. Jets are found in the magnetosheath and mostly form close to the bow shock. Some jets propagate through the magnetosheath and reach the magnetopause, where they can locally compress or disturb this boundary. Such interactions may have consequences for how energy is transferred into the magnetosphere.

Most observations of magnetosheath jets come from Earth's environment, primarily because it is closest and therefore easiest to probe with instruments onboard spacecraft. Numerous spacecraft missions provide measurements with good spatial and temporal coverage. However, similar plasma processes occur at other planets as well. Extending our understanding beyond Earth is therefore essential for developing a more universal description of solar wind–planet interactions. Although, we will give a general overview of magnetosheath jets, this thesis particularly focuses on the following questions:

- How do magnetosheath jets propagate through the magnetosheath and interact with the ambient plasma?
- How do jets interact with the magnetopause and what are the subsequent effects on the magnetosphere?
- How do jets behave in other plasma environments?

2 Although, it is not the solar wind particles that directly cause northern lights, but a chain of processes lead to auroral display.

We study these questions by combining data from instrument onboard spacecraft with numerical simulations.

This thesis is organized to progressively build the necessary background and address these questions. Chapter 2 introduces the fundamental concepts of plasma physics, followed by a description of solar wind–planet interactions in Chapter 3. The current understanding of magnetosheath jets is then summarized in Chapter 4. Chapter 5 and Chapter 6 describe the observational and numerical methods used in this work. The main results of each paper included in this thesis are presented in Chapter 7, and finally, Chapter 8 provides a summary and outlook for future research.

2 BASIC SPACE PLASMA PHYSICS

In this section, we define what a plasma is and introduce the mathematical tools used to describe it throughout this thesis. The presentation is based on the textbook by Baumjohann et al. (2012), which also provides a broader and more general overview.

2.1 WHAT IS A PLASMA?

As space is filled with plasma, we start with defining what a plasma[1] is and how to describe it mathematically to predict and understand its behavior. A plasma is the fourth state of matter in which charged particles move freely while maintaining quasi-neutrality, meaning that within a sufficiently large volume, the amounts of positive and negative charge are approximately equal. For the particles to move freely, their random kinetic (thermal) energy must be higher than electrostatic potential from neighboring particles. That is, that large scale magnetic and electric fields will dominate the motion of particles rather than other charges nearby.

For a plasma to appear electrically neutral the typical scales of a system needs to be larger than the distance for a test charge to be shielded. To put this in a more mathematical description, the potential from a test charge decreased by e^{-1} at a distance given by the Debye length

$$\lambda_D = \sqrt{\frac{\epsilon_0 k_b T_e}{n_e q^2}}, \tag{2.1}$$

where ϵ_0 is the vacuum permittivity, k_b is Boltzmann constant, T_e is the electron temperature, n_e is the electron density, and q the elementary charge. In order for Debye shielding to be effective, enough particles needs to be in a sphere with radius λ_D. This second criterion defines the plasma parameter

$$\Lambda = n_e \lambda_d^3 \gg 1. \tag{2.2}$$

The third criterion concerns the time scales of a plasma. If a plasma is locally disturbed, the electrons[2] react by oscillate around their equilibrium position with frequency

$$\omega_{pe} = \sqrt{\frac{n_e q^2}{m_e \epsilon_0}}, \tag{2.3}$$

1 Blood plasma is not a plasma in a physical sense, but a liquid.

2 Electrons are much lighter so they can react much quicker

where m_e is the electron mass. In a plasma, collisions should not dominate the behavior and therefore the plasma frequency ω_{pe} should be much larger than the collision frequency with neutrals τ_n such that

$$\omega_{pe}\tau_n \gg 1. \tag{2.4}$$

2.2 MATHEMATICAL DESCRIPTION OF A PLASMA

There are different ways to investigate how a plasma behaves. One of them is to consider the movement of a single charged particle in spatially and temporally varying electric field $\mathbf{E}(\mathbf{x}, t)$ and magnetic field $\mathbf{B}(\mathbf{x}, t)$. The force on a particle with charge q and mass m can in the non-relativistic limit[3] be expressed as

$$\mathbf{F} = m\frac{d\boldsymbol{v}}{dt} = q(\mathbf{E} + \boldsymbol{v} \times \mathbf{B}), \tag{2.5}$$

where $\boldsymbol{v}$ is the particles velocity. This equation describes that a charged particle with non-zero velocity in a constant magnetic field will have a circular motion in the plane perpendicular to the background magnetic field. This motion is the gyromotion and its frequency ω_g is determined by

$$\omega_g = \frac{|q|\mathbf{B}}{m}, \tag{2.6}$$

with electrons and ions gyrating in opposite directions.

However, the movement of a single particle does not explain the full picture of particle dynamics in space plasma physics, since the collective behavior of charged particles dominate the dynamics in a plasma. It is therefore useful to instead of describing a single particle to describe many particles using a particle distribution function $f(\mathbf{r}, \boldsymbol{v}, t)$ which essentially describes how many particles have the approximately velocity $\boldsymbol{v}$ close to point $\mathbf{r}$ at time t. This description of a plasma is the *kinetic* description of a plasma. The particle distribution function f does not tell us much about physical quantities of the plasma like the density and bulk flow $\boldsymbol{v}_b$, these can be easily obtained by integrating over the particle distribution function

$$n(\mathbf{r}, t) = \int f(\mathbf{r}, \boldsymbol{v}, t) d\boldsymbol{v} \tag{2.7}$$

$$\boldsymbol{v}_b(\mathbf{r}, t) = \frac{1}{n}\int \boldsymbol{v}\, f(\mathbf{r}, \boldsymbol{v}, t)\, d\boldsymbol{v}. \tag{2.8}$$

Furthermore, the pressure tensor can be calculated as follows

$$\mathbf{P} = m\int (\boldsymbol{v} - \boldsymbol{v}_b) \cdot (\boldsymbol{v} - \boldsymbol{v}_b) f(\mathbf{r}, \boldsymbol{v}, t)\, d\boldsymbol{v}. \tag{2.9}$$

3 This thesis discusses plasma environments close to Earth and Mars that can be treated non-relativistically. One exception are the radiation belts where electrons can be found moving at relativistic speeds, however, radiation belt particles are not discussed in this work.

The pressure tensor can be used to calculate the *kinetic* temperature[4] using $p = 3nk_bT$ where p is the trace of the pressure tensor. Sometimes, it can be also useful to define two temperature components, one parallel to the magnetic field $T_{\parallel}$ and one perpendicular to the magnetic field $T_{\perp}$.

The particle distribution describes the exact position and velocity of each particle in space at a given time t[5]. This approach is used in kinetic simulations where physical quantities like the density and velocity are extracted from the particles in a simulation[6], this is discussed in more detail in Chapter 6. Often it is however more useful to represent the particle distribution function as a mathematical function which represents an *ensemble-average phase space density*. Most of the time one is especially interested in the velocity distribution function $f(\boldsymbol{v})$ at a certain point $\mathbf{r}_0$ in space at time t_0 (so $f(\boldsymbol{v}) = f(\boldsymbol{v}, \mathbf{r}_0, t_0)$). If the plasma is in a thermal equilibrium, the velocity distribution function can be represented by a Maxwellian velocity distribution function. The evolution of the phase space density for collisionless plasmas[7] is described by the Vlasov equation

$$\frac{df}{dt} = \frac{df}{dt} + \boldsymbol{v} \cdot \nabla_{\mathbf{r}} f + \frac{q}{m} (\mathbf{E} + \boldsymbol{v} \times \mathbf{B}) \cdot \nabla_{\boldsymbol{v}} f = 0. \tag{2.10}$$

Another approach is the *magnetohydrodynamic description* which describes a plasma as an electrically conducting fluid using macroscopic quantities like the density and velocity. Instead of describing the system with phase space densities, only macroscopic quantities are used. By integrating moments of Equation (2.10) over velocity space one can derive a set of conservation laws for each particle species, this is the *multi-fluid* theory. Since it can be convenient to treat a plasma as a single fluid, by combining the densities and velocities of electrons and ions, n_i, n_e, $\boldsymbol{v}_i$, and $\boldsymbol{v}_e$ into a single components n and v. The resulting equations are the *magnetohydrodynamic equations* describing the conservation of mass, momentum, and energy. The continuity equation describes the conservation of mass

$$\frac{\partial n}{\partial t} + \nabla \cdot (n\boldsymbol{v}) = 0, \tag{2.11}$$

and the equation of motion describes the conservation of momentum,

$$\frac{\partial (nm\boldsymbol{v})}{\partial t} + \nabla \cdot (nm\boldsymbol{v}\boldsymbol{v}) = -\nabla \cdot \mathbf{P} + \rho\mathbf{E} + \mathbf{j} \times \mathbf{B}, \tag{2.12}$$

4 The kinetic temperature is only similar to the temperature in thermodynamics if the plasma is close to thermal equilibrium.

5 Mathematically, this corresponds to a sum of Dirac delta functions each representing one particle with a certain velocity and position at time t

6 Due to the extremely large number of particles in a plasma, it is not feasible for simulations to treat each particle as a single electron or ion. Tracking every individual particle would be computationally impractical. Instead, each simulated particle typically represents an ensemble of many real particles.

7 Most plasma environments discussed in this thesis can be treated in the collisionless limited with the exception of the ionosphere (upper ionized part of the atmosphere).

where $\rho = q(n_i - n_e)$ is the charge density, $j = q(n_i v_i - n_e v_e)$ is the current density, and $m \approx m_i$ is the mass which corresponds approximately to the ion mass. I don't like the explanation here going from the tensor to the scalar dynamic pressure. It has something to do with streamline which have constant pressure. The term $nmvv$ is the momentum flux and the trace nmv^2 acts like a pressure from the bulk movement of the plasma flow, this is the *dynamic pressure*[8], one of the key quantities in this thesis as it is used to define *magnetosheath jets*, the main topic of this thesis.

Each conservation law introduces a new variable which is defined by the next higher order equation, so the system of equations is not closed. To close the system of equations, an additional equation is needed. For example, an expression for the current density $\mathbf{j}$ is needed which was introduced by the momentum equation, Equation (2.12). The evolution of $\mathbf{j}$ is given by Ohm's law which for a single-fluid magnetohydrodynamic plasma is

$$\mathbf{E} + \boldsymbol{v} \times \mathbf{B} = \eta \mathbf{j} + \frac{1}{nq}\mathbf{j} \times \mathbf{B} - \frac{1}{nq}\nabla \cdot \mathbf{P}_e + \frac{m_e}{ne^2}\frac{\partial \mathbf{j}}{\partial t}, \tag{2.13}$$

where η is the plasma resistivity, and $\mathbf{P}_e$ is the electron pressure tensor. In an ideally conducting magnetohydrodynamic fluid all the terms of the right hand of Equation (2.13) side can be set to zero such that

$$\mathbf{E} + \boldsymbol{v} \times \mathbf{B} = 0, \tag{2.14}$$

which is ideal Ohm's law. When ideal Ohm's law is a good approximation to describe the plasma, the plasma is *frozen-in*, which means that the magnetic field and the plasma move together and are not separable entities.

Since in a plasma the particles act collectively, they can create magnetic and electric fields which in return change the trajectory of the particles, the particle motion and the electromagnetic fields are therefore coupled. This is described by the Maxwell equations (Maxwell, 1865)

$$\nabla \cdot \mathbf{B} = 0 \tag{2.15}$$

$$\nabla \cdot \mathbf{E} = \frac{\rho}{\epsilon_0} \tag{2.16}$$

$$\nabla \times \mathbf{B} = \mu_0 \mathbf{j} + \epsilon_0 \mu_0 \frac{\partial \mathbf{E}}{\partial t} \tag{2.17}$$

$$\nabla \times \mathbf{E} = -\frac{\partial \mathbf{B}}{\partial t}. \tag{2.18}$$

8 Typically, the dynamic pressure is defined as $\frac{nmv^2}{2}$ which is a term in the Bernoulli equation describing the conservation of energy. In classical fluid dynamics the dynamic pressure nmv^2, therefore represents the kinetic energy density while in magnetohydrodynamics the dynamic pressure is a momentum flux which is equivalent to a force acting per unit area. In Paper II we therefore use $0.5P_{dyn}$ to describe the kinetic energy density

Together with either the Vlasov equation or the magnetohydrodynamic equation they form a set of equations describing how plasma properties and the fields evolve in time.

Which description is appropriate depends on the problem at hand. In the magnetohydrodynamic description, different plasma components can not be separated, the velocity distribution should therefore be close to a Maxwellian. Furthermore, magnetohydrodynamics can only be used to describe processes at spatial and temporal scales larger than the scales of ions, described by the gyrofrequency ω_g and gyroradius $r_g = \frac{v_\perp}{\omega_g}$ with $v_\perp$ the speed perpendicular to the magnetic field. In contrary, kinetic processes become relevant at scales smaller than the electron inertial length

$$\delta_e = \frac{c}{\omega_{pe}}, \tag{2.19}$$

with c as the speed of light. Similarly, the ion inertial length δ_i can be defined using the ion plasma frequency ω_{pe}. At spatial scales smaller than the δ_e, a kinetic description is needed and at spatial scales larger than δ_i both electrons and ions behave like a fluid and therefore the fluid description is sufficient. The middle ground is at spatial scales larger than δ_e and smaller than δ_i, then electrons can be treated as a fluid but ions should be described with kinetic theory. This hybrid approach is used in this thesis for a numerical model described in Chapter 6.

2.3 WAVES IN PLASMAS

Waves are disturbances that transport energy and information. In everyday life, familiar examples include light, which is an electromagnetic wave in which electric and magnetic fields oscillate, and sound, which consists of compressional waves associated with small density variations in air. In plasmas, waves are also present, but their behavior is more complex because the electric and magnetic fields are coupled to the motion of the charged particles. This coupling gives rise to a wide variety of distinct wave modes. Waves in collisionless plasmas are of particular importance, as they provide an efficient mechanism for transporting and redistributing energy between particles[9]. For a wave to be excited, the plasma must be driven out of equilibrium. For example, a Maxwellian velocity distribution is considered to be stable, meaning that no waves are generated if all particle populations follow such a distribution.

In plasmas, wave properties, such as propagation speed and the physical quantities that oscillate, can be derived under appropriate assumptions. Typically, these derivations assume that the plasma is close to an

9 In solids, liquids, and gases, energy is mainly redistributed through collisions between particles. In collisionless plasmas, waves can play a similar role.

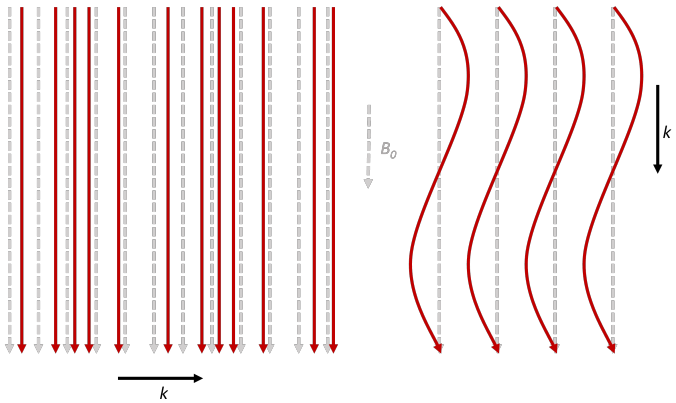

Figure 2.1: Illustration of the magnetic field disturbances (red) for the compressional modes (left) and the shear Alfvén mode (right). The undisturbed field in the background is shown in gray.

equilibrium state and that the perturbations are small compared to the *background* plasma conditions.

Because charged particles are influenced by the magnetic field, it is often useful to describe wave propagation and field perturbations relative to the background magnetic field. This is commonly achieved using a field-aligned coordinate system, in which one component is parallel ($\parallel$) to the magnetic field and the other two components are perpendicular ($\perp$) to it.

In the framework of ideal magnetohydrodynamics (MHD), and assuming a homogeneous background magnetic field and small-amplitude perturbations, three fundamental plasma wave modes arise: the *shear Alfvén wave*, the *fast magnetosonic wave*, and the *slow magnetosonic wave*.

The shear Alfvén wave can propagate along the magnetic field and, in this case, it travels at the Alfvén speed[10]

$$v_A = \frac{B}{\sqrt{\mu_0 n m}}. \tag{2.20}$$

The shear Alfvén wave is non-compressional, meaning that neither the magnetic field magnitude nor the plasma density changes during the wave propagation[11].

The fast magnetosonic wave is the only MHD wave mode that can propagate perpendicular to the background magnetic field. Unlike the Alfvén wave, it is compressional: both the magnetic field strength and

10 The Alfvén wave is non-dispersive so that the group and the phase velocity are the same.

11 The wave can be visualized as magnetic field lines oscillating sideways, similar to the vibration of a guitar string

the plasma pressure fluctuate in phase. For perpendicular propagation, the phase velocity is the magnetosonic speed

$$c_{ms} = \sqrt{v_s^2 + v_A^2}, \tag{2.21}$$

where $v_s = \sqrt{\frac{\gamma k_B T}{m_i}}$ is the sound speed, and γ is the polytropic index.For parallel propagation, the phase velocity of fast magnetosonic mode is v_A if $v_A > v_s$ or v_s if $v_s > v_A$.

The slow magnetosonic wave, in contrast, cannot propagate in the purely perpendicular direction. Instead, it propagates preferentially along the magnetic field and at lower speeds than the fast mode. In this case, fluctuations in magnetic field strength and plasma pressure are out of phase.

When the background magnetic field is not homogeneous, these fundamental magnetohydrodynamic wave modes can still be identified, but their properties are modified. This is the case for waves propagating in Earth's magnetosphere, which will be discussed in more detail in Section 3.1.

In Paper I, we identified several wave modes based on their observed properties, namely electrostatic solitary waves, electron acoustic waves, whistler waves, and lower hybrid waves. The electrostatic solitary waves and electron acoustic waves are both electrostatic in nature, meaning that their signatures are primarily observed in the electric field, with little or no corresponding magnetic field fluctuations. In contrast, whistler waves are electromagnetic waves that propagate predominantly along the magnetic field. They are right-hand circularly polarized and are known to efficiently transfer energy between the wave and resonant electrons (Jiang et al., 2024). We also identified waves consistent with lower hybrid waves. Although these waves are often described in the electrostatic limit, they can still exhibit magnetic field fluctuations (Norgren et al., 2012). Lower hybrid waves typically propagate nearly perpendicular to the background magnetic field, with electric field fluctuations mainly confined to the perpendicular plane. They can contribute to the broadening of density gradients and to the heating of cold ion populations (Graham et al., 2017). In addition to these identified wave modes, we also report two types of waves in Paper I that could not be clearly classified. Their properties do not match those of the standard textbook wave modes. Since theoretical wave properties are usually derived under simplifying assumptions, for example homogeneous magnetic fields or uniform plasma density, these discrepancies may indicate that such assumptions are not satisfied in the observed plasma conditions.

2.4 SHOCKS

When the plasma flow relative to an obstacle exceeds the speed of one of the fundamental magnetohydrodynamic (MHD) wave modes discussed in Section 2.3, a shock forms. This occurs because waves that would otherwise carry information about the presence of the obstacle cannot propagate upstream fast enough to influence the incoming plasma. Both the fast and slow magnetosonic modes can, in principle, steepen into shocks, separating upstream and downstream regions with different plasma densities, pressures, and velocities. In this thesis, we focus on fast magnetosonic shocks, as these are the types of shocks encountered in planetary plasma environments. Across a fast shock, the plasma is decelerated, while the density and magnetic field strength increase from upstream to downstream.

A useful parameter for determining whether a shock will form is the magnetosonic Mach number,

$$M_{ms} = \frac{v}{c_{ms}}, \tag{2.22}$$

where v is the plasma flow speed and c_{ms} is the magnetosonic speed. A shock forms when $M_{ms} > 1$.

In this thesis, we are particularly concerned with supercritical shocks. At such shocks, the dissipation mechanisms responsible for converting kinetic energy into thermal energy are not sufficient on their own to reduce the speed of the incoming plasma to subsonic values. As a result, additional processes are required, which leads to the reflection of incoming particles at the shock front. These reflected particles travel back upstream and drive the shock's structure and dynamics.

The behavior of these reflected particles depends strongly on the angle θ_{Bn} between the upstream magnetic field and the shock normal. If $\theta_{Bn} > 45°$, the shock is referred to as *quasi-perpendicular*. In this case, the reflected particles remain confined near the shock because their motion is tied to the magnetic field due to their gyration.

In contrast, for $\theta_{Bn} < 45°$, the shock is *quasi-parallel*. In this regime, reflected particles can escape far upstream along the magnetic field lines. As a result, the upstream region becomes populated by a mixture of incoming solar wind plasma and reflected particles. This coexistence of particles moving in different direction creates an unstable plasma environment, which drives the growth of waves and leads to a highly turbulent upstream region.

3

THE INTERACTION BETWEEN THE SOLAR WIND AND PLANETARY BODIES

In our solar system, the Sun acts as a natural source of plasma. It continuously emits a stream of plasma that expands throughout the solar system, known as the *solar wind*. Because the Sun's magnetic field is frozen into the solar wind, the expanding plasma carries this magnetic field with it into interplanetary space. This extended magnetic field is referred to as the *interplanetary magnetic field* (IMF). Due to the rotation of the Sun, the IMF, which is approximately radial close to the Sun, becomes twisted into a spiral structure known as the Parker spiral (Parker, 1958).

As the solar wind propagates through the solar system, it interacts with various planetary bodies. This chapter reviews the basic properties of the solar wind interaction with Earth (see Figure 3.1). The solar wind interaction with planets that lack an intrinsic dipole magnetic field, such as Venus and Mars, is also briefly discussed.

3.1 THE SOLAR WIND INTERACTION WITH EARTH

At Earth's orbital distance, the solar wind typically has a density of $5-10\,\mathrm{cm}^{-3}$, a bulk speed of about 400 km/s, and a magnetic field strength of $5-10\,\mathrm{nT}$[1] (Ma et al., 2020). Due to the Parker spiral configuration, the IMF is inclined at an angle of approximately 45° relative to the Sun–Earth line at this distance (Svalgaard et al., 1974).

When the solar wind reaches Earth's magnetic field, it does not penetrate directly into the atmosphere but is instead deflected around the magnetosphere. This interaction gives rise to the near-Earth plasma environment, illustrated in Figure 3.1. The main regions relevant to this thesis are the bow shock, the magnetosheath, the magnetopause, and the dayside magnetosphere.

The bow shock and the foreshock

The solar wind propagates at speeds much higher than the fast magnetosonic wave speed. Because of this supermagnetosonic flow and the presence of Earth's magnetic field acting as an obstacle, a shock front forms upstream of Earth, known as the bow shock. The average

1 For comparison, this density is comparable to the "strongest vacuum" achieved in a laboratory (Redhead, 1999) and the speed is faster than any manmade vehicle has achieved. As for the magnetic field, the Earth's magnetic field at the surface is about $30-60\,\mu\mathrm{T}$, i.e., roughly 1000 times stronger.

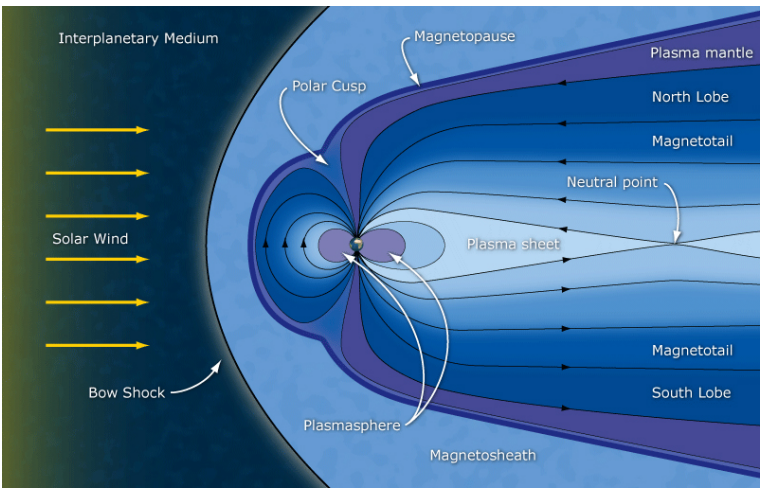

Figure 3.1: Schematic of various regions in the near Earth plasma environment that form as a result of the solar wind interacting with the Earth's magnetic field. Credits: ESA (original picture courtesy C. Russel)

stand-off distance of Earth's bow shock is approximately $15\,R_E$ (Fairfield, 1971), where $1\,R_E = 6371$ km is the mean radius of Earth.

Earth's bow shock typically has a magnetosonic Mach number of $M_{ms} \approx 8 - 10$ (Baumjohann et al., 2012), indicating that it is a fast magnetosonic shock. Across such a shock, both the plasma density and the magnetic field strength increase. As a result, the solar wind plasma is heated, compressed, and decelerated at the bow shock. The plasma density and the tangential component of the magnetic field increase by approximately a factor of four from the upstream to the downstream region of the shock, while the velocity component normal to the shock decreases by a similar factor. Consequently, the dynamic pressure is reduced by roughly a factor of four across the shock.

The bow shock is curved, as illustrated in Figure 3.1, which implies that both quasi-parallel ($0° < \theta_{Bn} < 45°$) and quasi-perpendicular ($45° < \theta_{Bn} < 90°$) regions always coexist along the shock surface. As discussed in Section 2.4, ions are reflected at the quasi-parallel bow shock (Thomsen et al., 1983) and propagate upstream along the magnetic field. The region upstream of the bow shock that is magnetically connected to it and populated by these backstreaming ions is referred to as the *foreshock* (Eastwood et al., 2005); see Figure 3.2.

These backstreaming ions interact with the incoming solar wind, leading to the growth of waves driven by a variety of plasma instabilities (Eastwood et al., 2005; Wilson, 2016). As these waves evolve, they can steepen into distinct foreshock structures, such as foreshock compressive structures (FCSs) (Suni et al., 2021), short large-amplitude magnetic structures (SLAMS) (Schwartz et al., 1991, 1992), and shocklets (Hoppe

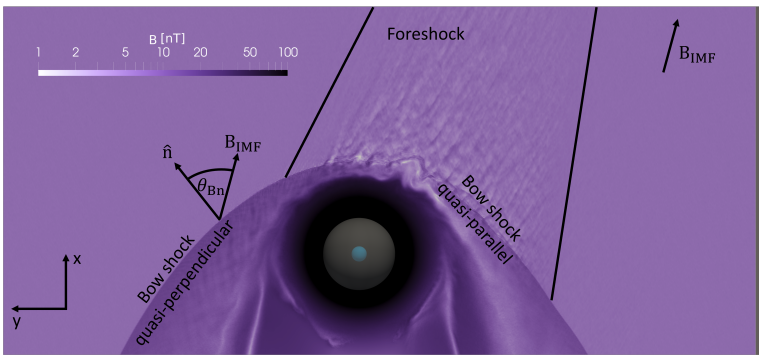

Figure 3.2: Simulated magnetic field strength in the near-Earth plasma environment in the equatorial plane. The quasi-perpendicular shock and the quasi-parallel bow shock are marked as well as the foreshock.

et al., 1981). FCSs are characterized by enhancements in both the magnetic field and the dynamic pressure (Suni et al., 2021), whereas SLAMS and shocklets primarily exhibit enhancements in the magnetic field, but differ in their relative amplitudes and spatial scales (Lucek et al., 2002). In addition to backstreaming ions and steepened waves, a range of transient structures can form in the foreshock, including hot flow anomalies, foreshock bubbles, and traveling foreshocks, which are generated by changes in the orientation of the IMF (Kajdič et al., 2024; Zhang et al., 2022).

The magnetosheath

The region downstream of the bow shock is the magnetosheath, which contains shocked solar wind plasma that is heated, compressed, and decelerated. In this region, the plasma is primarily deflected around the magnetosphere, the area dominated by Earth's magnetic field.

The plasma in the magnetosheath is highly fluctuating, but its properties differ depending on whether it is downstream of the quasi-parallel or quasi-perpendicular bow shock (Lucek et al., 2005). Accordingly, the magnetosheath is often divided into the *quasi-parallel magnetosheath*, which is magnetically connected to the quasi-parallel bow shock, and the *quasi-perpendicular magnetosheath*, which is connected to the quasi-perpendicular bow shock. Because the properties of the bow shock are determined by upstream solar wind and IMF conditions, the characteristics of the magnetosheath are also controlled by the bow shock regime (e.g. Lucek et al., 2005; Turc et al., 2020).

In general, the plasma quantities in the quasi-perpendicular magnetosheath are less fluctuating than the quasi-parallel magnetosheath (Lucek et al., 2005). In the quasi-parallel magnetosheath, transient en-

hancements in dynamic pressure, known as magnetosheath jets, are observed more frequently (Krämer et al., 2024; Plaschke, Hietala et al., 2018). These jets are the main subject of this thesis and will be discussed in greater detail in Chapter 4.

The magnetosphere

The magnetosphere is a region filled with plasma which is controlled by the Earth's magnetic field. Its outer boundary is the magnetopause and its inner boundary is the ionosphere, the upper part of the atmosphere ionized primarily by ultraviolet radiation from the Sun. While Earth's magnetic field is almost dipolar close to it's surface, the interaction with the solar wind deforms the dipolar shape: It is compressed on the side facing the Sun, *the dayside*, and is stretched out on the opposite side, the *nightside*, see the shape illustrated in Figure 3.1.

To describe the magnetic field configuration, several empical models have been developed, most notably the Tsyganenko models (e.g. Tsyganenko, 1989, 1995; Tsyganenko et al., 2005). These models are based on spacecraft observations and include contributions from key current systems, such as the magnetopause current, ring current, tail current, and field-aligned currents, as well as the penetration of the IMF into the magnetosphere. In Paper IV, the T96 model (Tsyganenko, 1995; Tsyganenko, 1996) is used to describe the magnetic field in the magnetosphere.

Magnetopause dynamics

On the dayside, the stand-off distance of the magnetopause at the subsolar point is primarily controlled by the solar wind dynamic pressure, which balances the magnetic pressure inside the magnetosphere. Under typical conditions, the magnetopause is located at a distance of about $10\,R_E$ (Cravens, 2004). However, the magnetopause interacts not with the pristine solar wind, but with the shocked plasma in the magnetosheath. In this region, much of the solar wind dynamic pressure has been converted into thermal pressure (Cravens, 2004), while magnetic pressure can also contribute to the total pressure acting on the boundary (Shue et al., 2013).

In addition, the orientation of the IMF plays an important role. A southward IMF can lead to magnetic reconnection at the magnetopause, causing erosion and an earthward motion of the boundary (e.g. Shue et al., 1998; Shue et al., 1997). Consequently, changes in solar wind dynamic pressure can lead to large-scale motion of the magnetopause.

Beyond these large-scale variations, transient pressure changes in the magnetosheath can produce localized magnetopause displacements. Such variations are often caused by dynamic structures, including magnetosheath jets (e.g. Kim et al., 2025; Němeček et al., 2023) and foreshock transients such as hot flow anomalies and foreshock bubbles (Grimmich

et al., 2023; Hartinger et al., 2013; Jacobsen et al., 2009). For example, the compressive edges of a hot flow anomaly can appear as jet-like dynamic pressure enhancements in the magnetosheath (Raptis et al., 2025; Zhou et al., 2024), while foreshock bubbles reduce the dynamic pressure, leading to local sunward bulges of the magnetopause (Archer et al., 2015).

However, the magnetopause does not respond instantaneously to such disturbances. Instead, it behaves as a low-pass filter: pressure variations must persist for several minutes in order to produce a significant boundary response, and the timescale of the magnetopause motion is typically longer than that of the driving disturbance (Archer, Horbury et al., 2013).

While foreshock transients and magnetosheath jets are mostly associated with magnetopause displacements on the dayside magnetopause close to the subsolar region[2], magnetopause displacement has also been associated with the Kelvin-Helmholtz instability (KHI) (Johnson et al., 2014). The Kelvin-Helmholtz instability can develop at the interface of two fluids moving at different velocities and can therefore develop at the magnetopause of planets since the magnetospheric plasma moves at slower speeds compared to the magnetosheath plasma at the flanks (Belmont et al., 1989). As the initial deformation grows, rolled up vortices form at the boundary which are a typical observation of the KHI in the nonlinear stage (Johnson et al., 2014). While the KHI can always grow in a fluid where a velocity shear is present, in a plasma, the compressibility of the plasma and magnetic shear leads to a stabilization of the KHI (Miura et al., 1982). In particular, if the magnetic field is parallel to the wave vector it has a stabilizing effects due to the magnetic tension force.

3.1.0.1 *ULF waves in the magnetosphere*

Inside Earth's magnetosphere, a wide variety of plasma waves occur, playing a crucial role in energy transport and particle dynamics. In this thesis, and in particular in Paper IV, we focus on ultra-low-frequency (ULF) waves in the Pc5 range. These waves have periods of $150 - 600\,\mathrm{s}$ and represent the lowest-frequency waves that the magnetosphere can sustain, as their wavelengths are comparable to the size of the system (Koskinen et al., 2022). On such large spatial scales, the wave modes can be discussed the magnetohydrodynamic limit, see Section 2.3.

For waves propagating along magnetic field lines, Earth's magnetic field acts as a guiding field. Since these field lines are anchored in the Southern and Northern ionosphere, only specific wavelengths can be sustained. In particular, standing wave modes can form when the wavelength matches $2l/n$, where l is the length of the magnetic field

2 Jet research has been focusing on the subsolar/dayside magnetosheath due to a spacecraft orbit bias. In addition, due to the higher magnetosheath flow at the flank/nightside magnetopause, it is expected that jets impact the nightside magnetopause less frequently, if at all.

line and n is an integer. These standing oscillations are known as field-line resonances.

Because the background magnetic field varies significantly on global scales, a local field-aligned coordinate system is used to describe the wave properties. In this system, the directions are defined as radial (outward from Earth), azimuthal (east–west), and field-aligned (parallel to the background magnetic field). Within this framework, ULF waves are commonly categorized into toroidal and poloidal modes. The toroidal mode corresponds to shear Alfvén waves, with perturbations in the azimuthal magnetic field and an electric field polarized in the radial direction. These waves propagate primarily along magnetic field lines. In contrast, the poloidal mode is associated with the fast magnetosonic mode, which can propagate across field lines. In this case, the electric field is oriented in the azimuthal direction, while magnetic field perturbations may be radial (for parallel-propagating poloidal modes) or field-aligned in the compressional mode.

In addition to their polarization, ULF waves are often characterized by their azimuthal wave number m, which describes how many wave cycles fit around Earth. Low-m waves ($m < 10$) are typically driven by externally and tend to exhibit a more toroidal polarization. For example, pressure disturbances compress the magnetosphere or launch fast-mode waves into the magnetosphere. When the frequency matches the eigenfrequency of a field-line and the local Alfvén speed, a perpendicular propagating wave can efficiently couple to a field-aligned propagating Alfvén wave which corresponds to a toroidal wave. This mechanism is particularly relevant for Paper IV as we study jet-driven disturbances and their associated Pc5 wave signatures in the ionosphere. In contrast, poloidal modes are more often associated with internal magnetospheric processes and frequently exhibit higher azimuthal wave numbers (Menk, 2011). (More citations?)

3.2 SOLAR WIND INTERACTION WITH UNMAGNETIZED PLANETS

Venus and Mars provide natural laboratories for studying solar wind interactions with planets that lack a global intrinsic magnetic field but possess a substantial atmosphere[3]. In the absence of a planetary magnetic field, it is the ionized atmosphere that forms the primary obstacle to the solar wind.

The upper part of the atmosphere becomes ionized due to photoionizaiton caused by the Sun's solar ultraviolet radiation, producing an ionosphere. This ionized region thus presents an obstacle to the solar wind (Cravens, 2004). The solar wind dynamic pressure is converted into magnetic pressure in the magnetosheath due to magnetic field

3 Mars has localized crustal magnetic fields that locally influence the interaction with the solar wind (Brain et al., 2003). Consequently, the solar wind interaction with Mars is sometimes considered hybrid. Since Paper V discusses magnetosheath jets in a global context, the Martian magnetosphere is introduced here as being in a purely induced state.

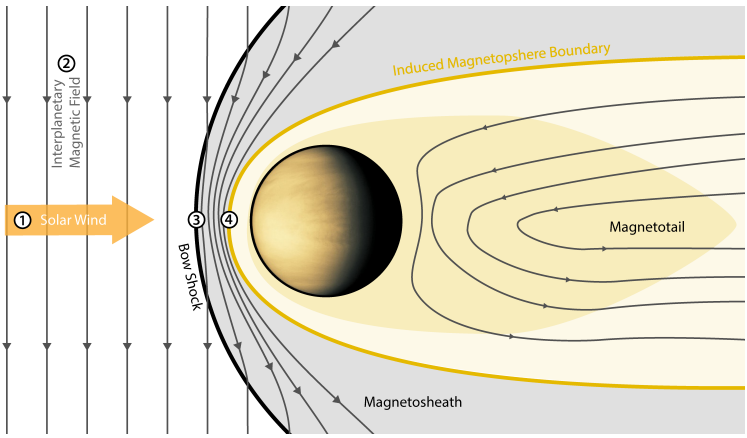

Figure 3.3: Overview over the plasma environment at Venus showing the direction of the solar wind flow (1), the IMF (2), the bow shock (3), and the induced magnetopause boundary (4). Figure by Albers et al. (2024), licensed under CC BY 4.0.

pileup. The magnetic pressure then balances the thermal pressure of the ionosphere and leads to the formation of an *induced magnetosphere*. A schematic of the solar wind interaction with an unmagnetized planet is shown in Figure 3.3, illustrating the Venusian plasma environment.

Despite the lack of an intrinsic magnetic field, the solar wind interaction at Mars and Venus shares several similarities with that at Earth. In all cases, the solar wind is super-magnetosonic, which leads to the formation of a bow shock upstream of the planet, followed by a magnetosheath region. However, the bow shock stand-off distances are much smaller: approximately 1.6 R_M (Martian radius, 1 R_M=3397 km) at Mars (Edberg et al., 2008) and 1.4 R_V (Venusian Radius, 1 R_V=6051 km) at Venus (Shan et al., 2015), compared to the terrestrial bow shock stand-off distance of about 15 R_E. This difference is primarily due to the smaller size of the obstacles, and as a consequence, the magnetosheath is also considerably thinner.

The bow shock structure at induced magnetospheres can also differ qualitatively from that at Earth. In particular, when the IMF is aligned with the solar wind flow direction (a *radial IMF*), magnetic field pileup in the magnetosheath is strongly reduced. Under such conditions, the bow shock can degenerate (Zhang et al., 2024). Additionally, because the bow shock is located so close to the planet, the extension of the neutral atmosphere, *the exosphere*, extends beyond the bow shock. Once exospheric atoms upstream the bow shock become ionized, they form a population of slow-moving ions compared to the solar wind speed. These ions can excite plasma waves upstream of the bow shock (Futaana et al., 2017; Zhang et al., 2025) in a similar manner than the reflected ions at the quasi-parallel shock. At Mars, it has therefore been pro-

posed that such upstream wave activity can influence the bow shock on a global scale, rather than being limited to the quasi-parallel shock geometry (Zhang et al., 2025).

The outer boundary of an induced magnetosphere is the Induced Magnetosphere Boundary (label 4 in Figure 3.3) which separates solar wind plasma from planetary plasma similar to the magnetopause at Earth. Crossing this boundary is associated with pronounced changes in several plasma parameters, including a change in magnetic field strength, enhanced magnetic field draping, electron temperatures decrease, and both the density and energy of solar wind ions are reduced (Bertucci et al., 2011). These observed changes are not necessarily co-located, and as a result, the terminology of this boundary varies throughout the literature depending on the observational criteria used to identify it (e.g. Matsunaga et al., 2017; Xu et al., 2016). In Paper V, we adopt the term *Induced Magnetopause Boundary* while we use *Induced Magnetosphere Boundary* in Paper VI.

4 MAGNETOSHEATH JETS

4.1 OVERVIEW

Magnetosheath jets are commonly defined as transient dynamic pressure enhancements in the magnetosheath. In simple terms, a jet is a plasma structure that moves faster and/or is denser than the surrounding plasma. An example observation of a magnetosheath jet is shown in Figure 4.1. For this particular event, both the plasma density (fourth row) and velocity (thrid row) are enhanced. In addition, the ion temperature is lower and more isotropic (fifth row), and the magnetic field strength is enhanced (second row). Reduced and more isotropic ion temperatures, together with enhanced magnetic fields, are typical features observed in magnetosheath jets (Plaschke et al., 2013; Raptis et al., 2020).

is typically?

Identifying jets in observational or simulation data requires the use of threshold-based criteria. These thresholds can be defined either relative to upstream solar wind dynamic pressure or relative to a local background value, typically computed using a running average (see discussion in Plaschke, Hietala et al., 2018). Criteria based on upstream solar wind conditions are motivated by the expectation that the solar wind dynamic pressure is reduced by approximately a factor of four across the subsolar bow shock at Earth (Hietala et al., 2024; Plaschke, Hietala et al., 2018). Because the solar wind velocity is predominantly directed along the Sun–Earth line, the largest velocity change across the subsolar bow shock occurs in the v_x component. For this reason, jets are often identified using the dynamic pressure

The jet selection criteria stems originally from observational studies and have thereafter been adapted to simulations. If you use virtual spacecraft in simulations, you can use very similar methods but in Shanab's first jet paper, he used something quite different

Well running average are usually used for observed data while you do something else in simulation data

Think about whether or not it is relevant to talk about observational and simulation studies in a different way, and if you change, change elsewhere accordingly.

$$P_{dyn,x} = mnv_x^2, \tag{4.1}$$

with a threshold $P_{dyn,x} > 0.5\,P_{dyn,sw}$. However, this criterion is only valid in the subsolar magnetosheath. In the original definition by Plaschke et al. (2013), an additional requirement was imposed: the v_x component has to be negative (moving anti-sunward) and remain enhanced over one-minute intervals before and after the event, ensuring that the structure has an anti-sunward flow enhancement.

Should you tell why?

Have you introduced your coordinate system for xyz?

An alternative approach is to define jets relative to the local background dynamic pressure. In this case, the background is typically computed using a running average over a time interval longer than the characteristic duration and recurrence time of jets. The original criterion uses an averaging interval of 20 minutes (Archer and Horbury, 2013). Shorter averaging intervals have also been employed (e.g. Mohammed-Amin et al., 2025; Raptis, Karlsson, Vaivads, Pollock et al., 2022; Suni

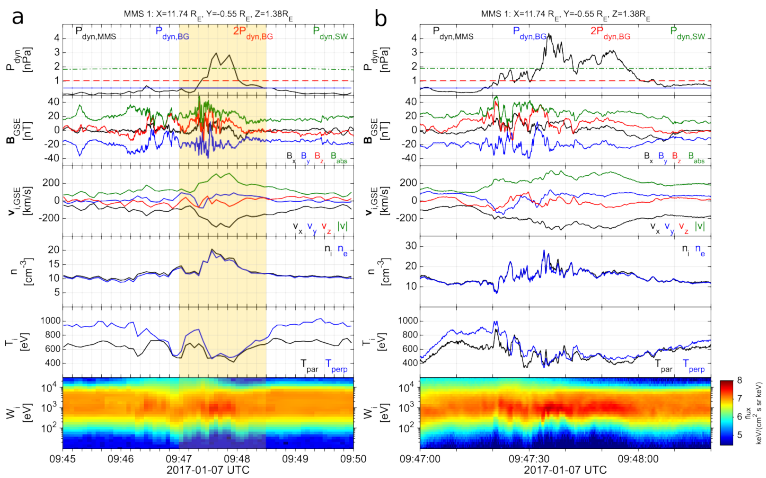

Figure 4.1: Jet observation by the MMS1 spacecraft. Left: Measurements at nominal time resolution (fast mode data). Right: Higher time resolution measurements (burst mode data) during the yellow-shaded interval indicated on the left. From top to bottom: Dynamic pressure and different thresholds derived from either upstream measurements or local background estimates, magnetic field, velocity, ion and electron number density, parallel and perpendicular temperatures (relative to the magnetic field), and differential ion flux. Reproduced from Krämer et al. (2024), licensed under CC BY 4.0.

After now having read some of your chapters, I wonder if your paragraphs (some of them) are a bit too long. Perhaps some of them would benefit from being split into two?

et al., 2021), for example in simulations with limited run times or in studies of jets downstream of other planetary bow shocks.

The use of different jet identification criteria leads to the identification of different plasma structures (Plaschke, Hietala et al., 2018), which also complicates direct comparisons between studies. In Papers I and IV, we used a background-based criterion, as some of the jets studied in Paper I were not observed in the subsolar magnetosheath. Papers II and III are based on simulations, where upstream solar wind parameters are well defined; in these cases, jets are identified through comparison with upstream values, without requiring velocity enhancements in the one-minute intervals before and after the jet. This criterion was chosen for consistency with Fatemi et al. (2024a) who investigated jets using the same plasma model and to avoid difficulties when computing running averages at non-stationary boundaries. In Paper II, we additionally consider P_{dyn} instead of $P_{dyn,x}$, as the use of $P_{dyn,x}$ was found to overestimate the disappearance rate of jets in the magnetosheath. In Paper V, we again employ a background-based criterion due to the lack of an upstream monitor at Mars and use 10-minute running averages, reflecting the comparatively thin magnetosheath.

If I were a reviewer, I would ask why

The overview presented here is primarily based on observations in the near-Earth plasma environment, where jets have been most extensively studied (e.g. Krämer et al., 2024; Plaschke, Hietala et al., 2018). Although the work presented in this thesis focuses on the propagation and effects of magnetosheath jets, we begin by discussing the proposed formation mechanisms of jets in Section 4.2. This is followed by a discussion of their propagation through the magnetosheath (Section 4.3) and their interaction with the magnetosphere (Section 4.4). Jets in other plasma environments are discussed in Section 4.5.

Finally, it is worth noting that jet nomenclature varies across the literature (Plaschke, Hietala et al., 2018). Terms such as *high-speed jets* are used when a significant velocity enhancement is present (Plaschke et al., 2013), while *plasmoids* has been used to both identify structures with enhanced velocity (Gunell et al., 2014) or enhanced density (Karlsson et al., 2012). Throughout this thesis, the term *jet* or *magnetosheath jet* is used to describe transient dynamic pressure enhancements.

4.2 OCCURRENCE AND FORMATION OF JETS

Magnetosheath jets are observed more frequently downstream of the quasi-parallel bow shock (e.g. Archer and Horbury, 2013; Plaschke et al., 2013; Vuorinen et al., 2019) and tend to occur preferentially close to the bow shock (Plaschke et al., 2013; Vuorinen et al., 2019). This spatial distribution suggests that their formation is closely linked to the dynamics of the quasi-parallel bow shock and the foreshock region, although the exact mechanisms remain an active area of research (Krämer et al., 2024).

One of the earliest proposed generation mechanisms is *bow shock rippling*. In this scenario, local variations in the shock geometry lead to regions where the incoming plasma is less efficiently decelerated but still strongly compressed (Hietala et al., 2009, 2012, 2013). As a result, localized regions of enhanced dynamic pressure can form downstream of the shock. These ripples may themselves be generated by upstream structures such as SLAMS convecting toward the bow shock (Schwartz et al., 1991) or by hot flow anomalies (Savin et al., 2012).

Another generation mechanism involves the transmission of foreshock structures across the bow shock. Several studies have suggested that structures such as SLAMS and other compressive structures can penetrate or interact with the shock and subsequently evolve into magnetosheath jets (e.g. Karlsson et al., 2015; Suni et al., 2021). For example, Karlsson et al. (2015) proposed that small-amplitude SLAMS can pass through the bow shock and interact with larger structures, such as large-amplitude SLAMS or hot flow anomalies, effectively creating localized shock ripples and generating jets. Similarly, Palmroth et al. (2018) found that SLAMS can form magnetosheath jets after crossing the shock. A follow-up study identified foreshock compressive structures (FCSs), characterized by enhanced dynamic pressure and magnetic field strength, and showed that a large fraction of jets downstream of the quasi-parallel bow shock are associated with FCSs crossing the shock Suni et al. (2021). However, this interpretation is not unchallenged. Xirogiannopoulou et al. (2026) argued that foreshock structures may not be the dominant source of jets, as their occurrence rates do not consistently correlate with jet occurrence under varying solar wind conditions. Instead, they proposed that fluctuations in the upstream magnetic field can lead to cyclic bow shock reformation, allowing solar wind plasma to enter the magnetosheath with reduced deceleration and thereby generating jets (Raptis, Karlsson, Vaivads, Pollock et al., 2022). In Paper III, we investigate the connection between jets and upstream magnetic field structures with enhanced amplitudes.

While most jet formation mechanisms focus on quasi-parallel shock dynamics, discontinuities in the upstream IMF can also lead to jet formation. In particular, rotational discontinuities in the interplanetary magnetic field can generate large-scale pressure enhancements in the magnetosheath (Archer et al., 2012; Suni et al., 2025). These events may produce longer-lived and potentially more geoeffective jets compared to those formed at the quasi-parallel shock. Similarly, the compressive edges of hot flow anomalies can appear as magnetosheath jets downstream of the shock (Raptis et al., 2025). One of the events analyzed in Paper IV is associated with such an IMF rotation.

Although jets occur more frequently downstream of the quasi-parallel bow shock, they are also observed downstream of the quasi-perpendicular shock (Goncharov et al., 2020). In this region, the formation mechanisms appear to differ. For example, localized acceleration processes, such as

those associated with non-reconnecting current sheets or reconnection exhausts, can create jet-like structures, particularly in the less turbulent quasi-perpendicular magnetosheath (Kajdič et al., 2021). In addition, flux tubes originating in the quasi-parallel foreshock can extend into the quasi-perpendicular magnetosheath and produce jet-like signatures (Kajdič et al., 2021). Other phenomena can also produce signatures that meet jet identification criteria. For instance, mirror mode structures, characterized by magnetic dips and density enhancements, may be classified as jets if the density increase is sufficiently large (Kajdič et al., 2021). Similarly, gyrating ion populations near the bow shock can produce localized dynamic pressure enhancements (Vuorinen et al., 2023). Finally, bow shock ripples also exist, even though with smaller scale sizes, at the quasi-perpendicular bow shock (Johlander et al., 2016) which could also lead to jet formation (Raptis et al., 2020). In Paper III, we report jets downstream of the quasi-perpendicular bow shock that are likely associated with flux tubes connected to the quasi-parallel region. In contrast, the jets analyzed in Paper IV are observed close to the quasi-perpendicular bow shock and may instead be related to gyrating ions.

Can we talk about flux tubes in a turbulent plasma?

Mirror modes can also be density dips but then they won't classify as jets (so mirror modes is more than what you wrote)

4.3 PROPAGATION OF JETS

The preferential occurrence of jets close to the bow shock already suggests that they evolve and ultimately "disappear" as they propagate through the magnetosheath. Observational studies have estimated typical jet sizes to be on the order of 1 R_E (Goncharov et al., 2020; Plaschke et al., 2016). However, these estimates are biased toward larger structures. Accounting for this observational bias, Plaschke, Jernej et al. (2020) argued that the characteristic scale size of jets is closer to 0.1 R_E.

These size estimates generally assume that jets are coherent, isolated structures with relatively simple geometries (e.g. Plaschke et al., 2016). However, recent global simulations challenge this picture. Instead of isolated entities, jets appear as highly dynamic and interconnected structures embedded within the magnetosheath flow, forming a complex, filamentary network that has been described as a *honeycomb-like* structure (Fatemi et al., 2024a; Ren et al., 2024). An example of such a structure is shown in Figure 4.2, where the yellow and red regions in the magnetosheath (with the bow shock indicated by black points) correspond to those interconnected jets.

As jets propagate through the magnetosheath, they interact continuously with the surrounding plasma, leading to a gradual evolution of their properties (e.g. Goncharov et al., 2020; Palmroth et al., 2018; Plaschke, Jernej et al., 2020). Observations indicate that jets thermalize as they move away from the bow shock while their density, velocity, and magnetic field strength decrease and become more similar to those of the ambient magnetosheath plasma (Palmroth et al., 2018). As a con-

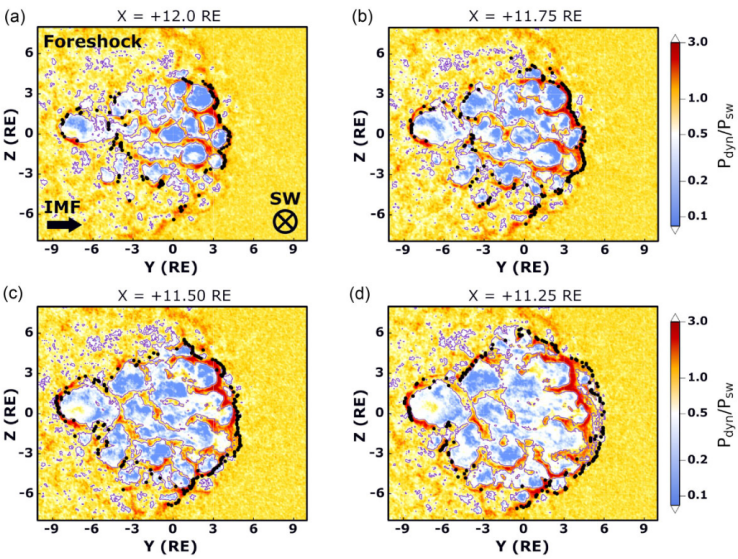

Figure 4.2: Relative dynamic pressure in four yz-planes showing the structure of jets. The black dots depict the bow shock and the contours give ?? around the yellow and red dynamic pressure enhancements depict magnetosheath jets. Reproduced from Fatemi et al. (2024a), licensed under CC BY 4.0.

sequence, the dynamic pressure within the jet decreases, reflecting a reduction in kinetic energy density. Jets can therefore be viewed as localized sources of kinetic energy that is redistributed within the magnetosheath. In Paper II, we quantify this energy conversion on global scales.

While it is clear that jets transfer energy to their surroundings, the main mechanisms responsible for this energy conversion are not yet fully understood. Several processes likely contribute. For example, supermagnetosonic jets can drive bow waves ahead of them (Karimabadi et al., 2014), which may lead to particle acceleration (Liu et al., 2019). In addition, the faster motion of jets relative to the ambient plasma can generate flow perturbations, accelerating plasma ahead of the jet and displacing it sideways, while a wake forms in the downstream region (Plaschke and Hietala, 2018). Another important aspect is the increased wave activity observed both inside jets and in their immediate vicinity (Gunell et al., 2014; Karlsson et al., 2018; Krämer et al., 2023). These waves may play a role in transferring energy between particles and fields. In Paper I, we use high time-resolution observations to identify wave modes within and around magnetosheath jets.

4.4 EFFECTS ON THE MAGNETOSPHERE

Some jets propagate all the way to the magnetopause and jets with scale sizes exceeding $2\,R_E$ are frequently found to impact the magnetopause, with an occurrence rate of approximately $2.4\,h^{-1}$ under average conditions and up to $7.9\,h^{-1}$ during low IMF cone angle conditions (Plaschke, Hietala and Vörös, 2020). When such jets reach the magnetopause, they can induce a range of responses by locally enhancing the dynamic pressure and thereby disturbing pressure balance at the boundary. These responses include magnetopause motion due to pressure imbalances (e.g. Escoubet et al., 2020; Hietala et al., 2009, 2012; Kim et al., 2025; Němeček et al., 2023; Shue et al., 2009), direct penetration of magnetosheath plasma into the magnetosphere (Gunell et al., 2012), and the triggering of magnetic reconnection through compression of the magnetopause (Hietala et al., 2018).

The jet-triggered magnetopause motion has often been studied using multi-spacecraft observations with separations of a few R_E. These measurements reveal large deformations of the magnetopause, including indentations of several R_E accompanied by simultaneous sunward bulges (Kim et al., 2025; Shue et al., 2009). Since multiple jets can impact the magnetopause at different locations simultaneously, the boundary can become dynamically disturbed during periods of enhanced jet occurrence (Escoubet et al., 2020), also shown in Figure 4.3. However, the magnetopause response is not purely instantaneous. Instead, it behaves similarly to a low-pass filter, smoothing out rapid variations and responding primarily to variations on timescales of several minutes. Con-

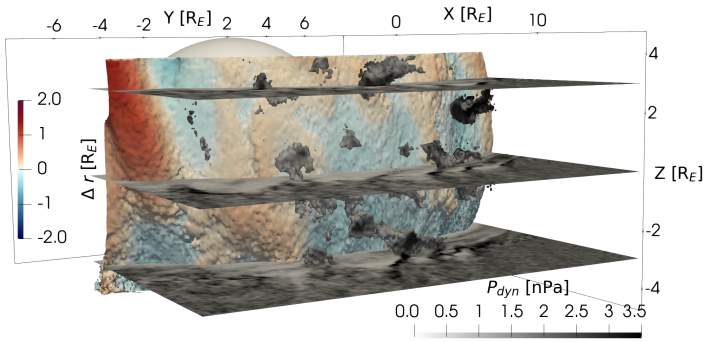

Figure 4.3: Disturbed magnetopause boundary (blue-red surface) interaction with jet (gray structures). Only jets within 8000 km of the magnetopause are shown. Reproduced from Cite paper III once published, hopefully, licensed under CC BY 4.0.

sequently, the magnetosphere might tend to respond to groups of jets rather than individual pulses (Archer, Horbury et al., 2013).

In light of recent observations of the interconnected and dynamic structure of magnetosheath jets, we further investigated magnetopause dynamics in response to jet impacts using three-dimensional simulations in Paper III. The jet interaction with the magnetopause in the simulation is shown in Figure 4.3 recovering a highly disturbed magnetopause. The simulation shows that continuous jet generation at the bow shock can drive flankward-propagating magnetopause surface waves (red bulge in Figure 4.3) due to continous jet impact at the magnetopause.

As a result of localized magnetopause deformations, jet impacts can also generate magnetospheric responses. In particular, electromagnetic waves in the Pc5 frequency range (with periods of $150-500$ s) have been observed both near the magnetopause and at geosynchronous orbit following jet impact (Archer, Horbury et al., 2013), as well as in ground-based magnetometer observations (Dmitriev et al., 2012; Norenius et al., 2021; Wang et al., 2022). These observations indicate that compressional disturbances at the magnetopause can excite ultra-low frequency (ULF) waves that propagate throughout the magnetosphere. The initial compressional perturbation can couple to field-aligned wave modes, allowing the disturbance to reach the ionosphere and be detected by ground-based instruments. Through this process, jets can transfer solar wind energy into the magnetosphere and the ionosphere.

The energy transported by these waves can contribute to ionospheric heating. For example, Rae et al. (2007) showed that sustained low-frequency wave activity over several hours can deposit up to 30% of the energy typ-

ically associated with a substorm[1]. Motivated by this, we estimated the contribution of jets to ionospheric energy input via Joule heating in Paper IV. Our results indicate that, although detectable, the contribution from jets is small compared to events like substorms.

I don't know if this is good

In addition to wave-driven effects, jet impacts have also been associated with diffuse and discrete auroral brightenings (Wang et al., 2018). The intensity of diffuse aurora has been suggested to be directly controlled by the dynamic pressure at the magnetopause (Wang et al., 2018), while discrete aurora can be driven by field-aligned electric fields associated with low-frequency wave activity, which accelerate particles into the ionosphere (Qiu et al., 2024). In Paper IV, auroral emissions were also observed during the investigated event. However, variable cloud coverage prevented a reliable assessment of changes in auroral intensity. Enhanced auroral activity would increase the overall energy input into the ionosphere. Nevertheless, even if this contribution is comparable to that from Joule heating driven by ULF waves, the total energy input associated with jets remains relatively small.

4.5 JETS IN OTHER PLASMA ENVIRONMENTS

Since jet formation is often associated with processes at the (quasi-parallel) bow shock, it is reasonable to expect that jets may also form downstream of other shock environments. While jets in the terrestrial magnetosheath have been extensively discussed in the literature, observations of jets downstream of non-terrestrial shocks have only recently been reported (Gunell et al., 2023; Hietala et al., 2024; Zhou et al., 2024). Specifically, Gunell et al. (2023) identified three jets downstream of the Martian bow shock, while Zhou et al. (2024) reported three jet events in Jupiter's magnetosheath. In addition, even interplanetary shocks characterized by lower Mach numbers and smaller compression ratios have been shown to produce dynamic pressure enhancements (Hietala et al., 2024).

To understand how dynamic pressure enhancements behave across different plasma environments, statistical studies are required; however, such studies are limited by the relatively small number of accessible environments. One option is to use data from the MAVEN spacecraft (Jakosky et al., 2015), which orbits Mars and provides extensive coverage of the Martian magnetosheath. We therefore study dynamic pressure enhancements downstream of the Martian bow shock in Paper V. The results were compared with jets observed in the terrestrial magnetosheath. However, this comparison is not straightforward, as MAVEN's highly inclined orbit causes it to sample the flank magnetosheath much more frequently than the subsolar region. This

1 A substorm is a transient disturbance in the Earth's magnetosphere during which stored magnetic energy on the nightside is rapidly released and injected into the ionosphere causing, for example, auroral display.

is further complicated by the restricted field of view of the instrument measuring plasma density and velocity which compromises the data quality. Therefore, this data in the subsolar region is often excluded to ensure sufficient data quality for statistical studies. Despite these challenges, we find that the Martian dynamic pressure enhancements exhibit overall behavior similar to terrestrial magnetosheath jets, although they occur on smaller spatial scales. Overall, those recent findings suggests that jet formation is not unique to Earth's magnetosheath, but is a universal process at shocks.

Also lack of upstream monitor complicates

5

SPACECRAFT MISSIONS AND GROUNDBASED MEASUREMENTS

To learn about magnetosheath jets and the plasma environment around planetary bodies we use measurements from instruments mounted on spacecraft. Since magnetic field line are connected to the ionosphere, even measurements on the ground can be used to infer the state and processes in the magnetosphere. In this chapter, we start with introducing the different space missions with the associated instrumentation, we then introduce ground based experiments.

5.1 THE MAGNETOSPHERIC MULTISCALE MISSION

To detect jets in the magnetosheath, we primarily use the Magnetospheric Multiscale (MMS) mission (Burch et al., 2016) consisting of four identical, spin-stabilized spacecraft that have been orbiting Earth in a highly elliptical orbit since 2015. An artistic impression of the four MMS spacecraft orbiting the Earth's magnetosphere is given in Figure 5.1. Its primary scientific objectives are to investigate the microphysics of magnetic reconnection at the dayside magnetopause and in the magnetotail neutral sheet. To achieve this, the spacecraft typically fly in a tetrahedral configuration with inter-spacecraft separations ranging from tens to hundreds of kilometers. The MMS mission not only enables high spatial resolution due to the small inter-spacecraft distance, but also high time resolution burst mode measurements. Burst mode measurements are only available for limited intervals due to telemetry limitations. Although the dayside magnetopause is one of the main region of interest, MMS data have also been widely used to study the foreshock, bow shock, and magnetosheath, including magnetosheath jets (e.g. Karlsson et al., 2018; Raptis et al., 2020; Raptis, Karlsson, Vaivads, Lindberg et al., 2022; Xirogiannopoulou et al., 2026). Each spacecraft carries instruments that measure magnetic and electric fields, as well as the particle distribution function which is used to derive parameters such as density and velocity.

We used MMS data in Papers I and IV. The mission concept discussed in Paper VI proposes instruments similar to those on the MMS spacecraft. When studying plasma structures that are typically much larger than the small MMS inter-spacecraft separations, such as magnetosheath jets, studies often rely primarily on data from one spacecraft only, e.g. MMS1 data, rather than on data from all four spacecraft. Accordingly, we mainly use data from MMS1, but in Paper I we also

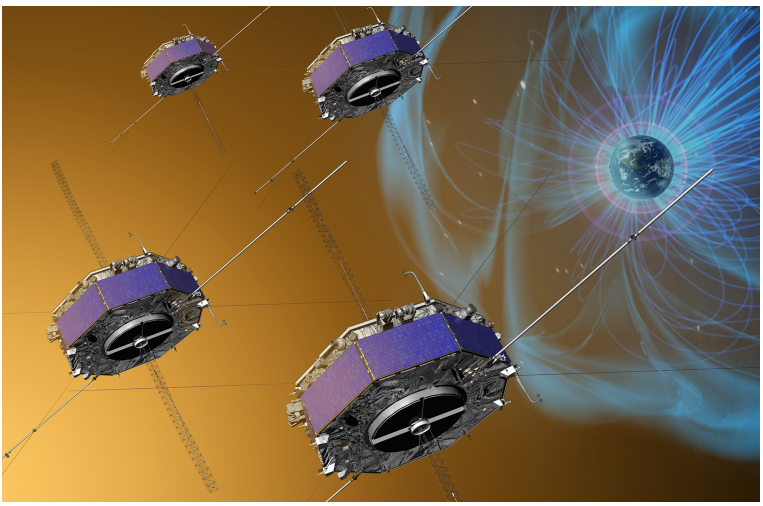

Figure 5.1: An artistic impression of the four MMS spacecraft in orbit around Earth's magnetosphere. Credits: NASA/GSFC

include MMS2–4 when analyzing the properties of electrostatic waves and computing the current based on Ampère's law.

Add figure with coordinate system Data from spacecraft measurements is presented in either Geocentric Solar Ecliptic (GSE) coordinates or Geocentric Solar Magnetospheric (GSM) coordinates if not stated otherwise[1]. In both coordinate systems x points toward the Sun. In the GSE coordinate system, z is parallel to the ecliptic pole, and y completes the right-hand coordinate system pointing toward dusk. In the GSM coordinate system, y is perpendicular to the magnetic dipole axis such that the xz-plane contains the dipole axis, and z completes the right hand coordinate system. Sometimes we also use a local field-aligned coordinate system,

In the following sections, we briefly introduce the instruments used in Papers I and IV.

Fast Plasma Investigation

Plasma properties like the density, velocity, and temperature can be derived using the Fast Plasma Investigation (FPI) instrument (Pollock et al., 2016). The FPI measures the differential directional flux of electrons and ions in the energy/charge range from 10 eV/q to 30 keV/q. In high-resolution (burst) mode, electron fluxes are sampled every 30 ms and ion fluxes every 150 ms, with a full 360° field of view. In regular time resolution (fast) mode, the fluxes are available every 4.5 s. In-

1 When studying waves it is sometimes more useful to use a local coordinate system aligned with the magnetic field, so called field-aligned coordinates.

stead of relying on the spacecraft's spin to achieve the high time resolution, the FPI uses four dual top-hat electrostatic analyzers mounted on each spacecraft. The angular resolution is 15° in the polar direction and 11.25° in the azimuthal direction.

Although the FPI instrument directly measures particle fluxes, these fluxes can be converted into velocity distributions. The resulting velocity distributions are then used to compute the moments of the velocity distribution, specifically, the number density, bulk velocity, and temperature for ions and electrons as described in Chapter 2. The FPI instrument does not differentiate between different ion species as it lacks a mass spectrometer.

Magnetic field measurements

Magnetic field measurements are provided by magnetometers. Each MMS spacecraft carries three magnetometers as part of the FIELDS instrument suite (Torbert et al., 2016), which together measure the magnetic field vector across a wide range of frequencies. Two redundant fluxgate magnetometers (Russell, Anderson et al., 2016) provide measurements from DC up to 64 Hz. In addition, a search-coil magnetometer (Le Contel et al., 2016) measures magnetic field fluctuations in the frequency range from 1 Hz to 6 kHz.

Electric field measurements

The electric field vector is derived from potential measurements by the spin-plane double probes (SDP) (Lindqvist et al., 2016) and the axial double probes (ADP) (Ergun et al., 2016) both of which are also part of the FIELDS instrumentation suite. The SDP consists of four identical probes placed on 60 m wire booms, separated by 90°, which measure the electric field in the spacecraft spin plane over a frequency range from DC to 100 kHz. The ADP measure the electric field along the spin axes, also covering the frequency range DC to 100 kHz. The two sensors included in the ADP are separated by 30 m. The electric field component E_{ij} between a pair of probes can be derived from the potential difference using

$$E_{ij} = -\frac{V_j - V_i}{d_{ij}}, \tag{5.1}$$

where V_i and V_j are the electric potentials measured by probe i and j, and d_{ij} is the distance between them.

Active spacecraft control

The MMS spacecraft also have the Active Spacecraft Potential Control (ASPOC; Torkar et al., 2016) onboard. The spacecraft potential is often

positive when the spacecraft is sunlit due to extreme ultra-violet radiation. To neutralize the spacecraft potential, the ASPOC releases positively charged ions. If the spacecraft potential is not neutralized, the trajectories of charged particles is influenced causing distorted particle distribution measurements. Furthermore, the electric field measurements are compromised. We propose the use of spacecraft potential control in our mission proposal in Paper VI with the MMS ASPOC as the heritage instrument.

5.2 THE TIME HISTORY OF EVENTS AND MACROSCALE INTERACTIONS DURING SUBSTORMS MISSION

The Time History of Events and Macroscale Interactions during Substorms (THEMIS; Angelopoulos, 2008) mission consists of five identical, spin-stabilized spacecraft launched in 2007, though two probes were relocated to orbits around the moon in 2010 forming the ARTEMIS mission (Angelopoulos, 2011). The objective of the THEMIS mission is to study the onset of magnetospheric substorms. The THEMIS carries, similar to MMS, scientific instruments to measure the plasma distribution as well as the magnetic and electric fields. In Paper IV we used the flux gate magnetometer (FGM Auster et al., 2008) for measurements of the interplanetary magnetic field upstream of the bow shock. The FGM provides the magnetic field vector with a measurement frequency of 64 Hz. We also used the FGM as a heritage instrument onboard the proposed mission to Venus described in Paper VI. In addition, we also used the electrostatic analyzer (ESA; McFadden et al., 2008) onboard the THEMIS spacecraft as a heritage instrument for our proposed mission to Venus. The ESA provides measurements of the ion and electron distributions each 3 s spin period in the energy range $1.6 - 25000$ eV for ions and $2 - 32000$ eV/q for ions. The field of view is 4π each spin.

5.3 THE HIGH-RESOLUTION OMNI DATASET

The OMNI dataset (Papitashvili et al., 2020) contains solar wind magnetic field and plasma data. This dataset is constructed using data from different space missions, in recent years mainly from ACE (Stone et al., 1998) and Wind spacecraft (Harten et al., 1995). Both spacecraft are orbiting Earth's Lagrange point 1. Since the solar wind takes on average about 1 hour from this Lagrange point to Earth, the data is then time shifted to the Earth's nominal bow shock nose. While the OMNI datasets on average give a good estimate of the solar wind conditions, the shift of the data to the bow shock introduces an temporal uncertainty (Case et al., 2012; Mailyan et al., 2008). The data is available at different time resolutions, in Paper I and IV we used the data with 1 minute cadence which is the highest available time resolution.

5.4 THE MARS ATMOSPHERE AND VOLATILE EVOLUTION MISSION

The Mars Atmosphere and Volatile Evolution (MAVEN; Jakosky et al., 2015) mission aims to study the Martian atmosphere. The spacecraft was launched in November 2013 and its science operation began in November 2014. The spacecraft is a three-axis stabilized spacecraft and the missions primary objective is to quantify the loss of atmospheric gas at Mars. The spacecraft is therefore equipped with full suite of plasma instruments. For our statistical study of jets in the Martian plasma environment in Paper V, we used two of the instrument on board the spacecraft, namely, the Solar Wind Ion Analyzer (SWIA; Halekas et al., 2015) and the fluxgate magnetometer (Connerney et al., 2015). SWIA is a top hat electrostatic analyzer with a $360° \times 90°$ build to measure the solar wind. The instrument has two modes, the coarse mode for the magnetosheath and the fine mode for the solar wind. There are also onboard plasma moments are calculated every 4 s which we use for our analysis. The magnetometer measures the magnetic field vector with a sampling frequency of 32 Hz.

5.5 GROUND-BASED MEASUREMENTS

Since the magnetosphere is magnetically connected to the ionosphere, measurements of the ionosphere can be complementary to space-bourne measurements. While it is difficult to probe the ionosphere directly with spacecraft, ground-based measurements can be used instead. In the following section, the ground-based instruments used in Paper IV, namely ground-based magnetometer, all-sky cameras, as well as coherent and incoherent scatter radars are introduced.

5.5.1 *Ground-based magnetometers*

Ground-based magnetometers measure the magnetic field vector on the ground. The magnetic field on the ground is the superposition of the Earth's internal magnetic field and external magnetic fields. The external magnetic fields are mainly the result of currents flowing in the ionosphere and magnetosphere giving rise to magnetic fields according to Amprère's law. Changes in the Earth's magnetic field are thought to be slow compared to changes in the ionospheric current systems, which can change on minute time scales. Therefore, the ionospheric contribution to the magnetic field measured on the ground can be approximated by subtracting a baseline magnetic field (e.g. Gjerloev, 2012). In addition to ionospheric currents, ground-based magnetometers can also be used to study low-frequency wave activity in the magnetosphere (e.g. Mathie et al., 2000; Murphy et al., 2011; Rae et al., 2007; Wang et al., 2022) as those waves cause magnetic disturbances in the ionosphere.

Ground-based magnetometers are usually operated by different organizations and national agencies using different data processing techniques. The worldwide collaboration SuperMAG (Gjerloev, 2009, 2012) provides data of ground magnetic field perturbations from nearly 600 magnetometers with a common data processing routine. Due to the easy data access and common data processing, we use SuperMAG data with 1 minute time resolution in Paper IV to determine the scale size of a disturbance in the ionosphere caused by a disturbance in the magnetosphere. SuperMAG data is given a local coordinate system with components B_N, B_E, and B_Z. With the N-component oriented toward local magnetic north, the E-component toward local magnetic east, and the Z-component is vertically down.

5.5.2 *All-sky cameras*

All-sky cameras are cameras that continuously take images of the night sky. They can be used to detect auroral display. While all-sky cameras generally do not measure a physical value (like the brightness of the auroral display which can be measured with photometers), they can be used to identify auroral display and track the motion of auroral structures. In Paper IV we examined changes in auroral display using an all-sky camera in conjunction with disturbances in the magnetic field associated with wave activity. In particular, we used the all-sky camera at the Kjell Henriksen Observatory on Svalbard (location in geographic coordinates: 78.148°N, 16.043°E, 520 m altitude).

5.5.3 *Radars*

Radars can be used to infer different plasma properties in the ionosphere, such as the electron density or line-of-sight flow velocity. Which properties can be measured depends on the radar type, and in particular the operating frequency. In Paper IV, we use data from both an incoherent scatter radar on Svalbard, EISCAT (Wannberg et al., 1997), and a coherent scatter radar, SuperDARN (Greenwald et al., 1995). The general working principle is the same for types: A radar consists of a transmitter, sending out electromagnetic waves and a receiver measuring the incoming power from a electromagnetic wave. The transmitter and the receiver can be the same antenna or two different ones. The basic idea behind a radar is that an electromagnetic wave is send out toward the ionosphere. In the ionosphere, certain plasma structures can scatter the transmitted wave, sending a small portion of the energy in the incoming wave in the direction of the receiver antenna. The signal is scattered when the Brag condition

$$2d \sin\theta = n\lambda_r, \tag{5.2}$$

is satisfied, with the scale length of the plasma density irregularities d, the angle of incidence θ, the diffraction index n, and the wavelength of the radar λ_r. The receiver then measures the properties of the incoming electromagnetic wave. The difference between an incoherent and a coherent scatter radar are the size of the plasma density irregularities they scatter on.

SuperDARN

The Super Dual Auroral Radar Network (SuperDARN) is an international network of coherent scatter radars (Greenwald et al., 1995) operating at frequencies between $8-20$ MHz. Coherent scatter radars scatter the signal from electron density fluctuations with scale sizes of several meters. Each radar can be used to estimate the line-of-sight drift velocity of the ionospheric plasma based on the Doppler shift of the received signal. Combining measurements from multiple radars allows the construction of convection maps at auroral latitudes, showing the ionospheric plasma convection.

In paper IV we use SuperDARN data to get an estimate of the electric field disturbance E in the ionosphere using that the drift velocity $v_d \sim E \times B$.

EISCAT

The European incoherent scatter (EISCAT) Svalbard radar (Wannberg et al., 1997) operates at 500 MHz and can infer electron density, the ion drift velocity, as well as electron and ion temperatures. Incoherent scatter radars scatter at smaller density fluctuations compared to incoherent scatter radars with length of less than a meter, hence the larger operating frequency.

In paper IV we use the EISCAT radar together with NRLMSIS atmospheric model (Picone et al., 2002) for an estimate of the height integrated ionospheric Pedersen conductivity.

6 NUMERICAL MODELS

6.1 NUMERICAL MODELS IN SPACE PLASMAS

In addition to spacecraft measurements, numerical models are frequently used to advance our understanding of plasma environments due to the complexity of interaction between the incident plasma and the body itself. Using simulations based on these numerical models has the advantage that the input parameters can be controlled and can provide a 2D or 3D view of a phenomena. Ideally, one would like to simulate all particle species using realistic masses and scales, however this is computationally not possible. Therefore, different modeling approaches, including magnetohydrodynamic (MHD) models, test particle simulations, kinetic particle-in-cell (PIC) models, Vlasov models, and hybrid models, have been developed (e.g. Büchner, 2005; Lapenta, 2016; Ledvina et al., 2008). Each model has its own set of assumption, advantages, and disadvantages. Which model should be chosen depends therefore on the phenomena of interest and in particular its scale size.

6.1.1 *MHD models*

MHD models describe the plasma as a conducting fluid, most commonly a single fluid approach is used, but there are even multi-fluid MHD models. The basis of MHD models are the fluid equations describing the conservation of mass, momentum, and energy expanded by the induction equation describing how electromagnetic forces act on the fluid. MHD models reproduce large scale plasma flows and are of use when the individual particle motion is not of interest. The simplest MHD model, the ideal MHD model, describes the plasma as a single, conducting fluid and the evolution of the magnetic field B is described by the magnetic induction equation, $\partial B/\partial t = \nabla \times (v \times B)$, where v is the plasma velocity. Expansions of the ideal MHD model, include multi-species or multi-fluid approaches or additional terms in the induction equation, in particular, Hall- and resistive terms. MHD models have been frequently used to study the global interaction between the solar wind and the Earth magnetic field (Wang et al., 2013). Due to the lack of ion kinetics, MHD models cannot self-consistently reproduce mesoscale feature such as the foreshock and magnetosheath jets.

6.1.2 *Test particle models*

Test-particle simulations incorporate limited kinetic effects by following the trajectories of individual particles (electrons or ions) through electromagnetic background fields. These background fields are typically obtained either from another simulation, for example, a global MHD or hybrid simulation, or from an analytical solution. Each test particle is treated independently, and its motion is governed by the electromagnetic forces acting upon it. There is no feedback from the test particles to the background fields, nor any interaction among the test particles themselves. Test-particle simulations are therefore most appropriate when the influence of particle motion on the background fields is negligible and when wave–particle interactions can be ignored.

6.1.3 *Kinetic models*

Fully kinetic models are generally implemented either as particle-in-cell (PIC) simulations or as Vlasov simulations. PIC models represent both electrons and ions as macro-particles, where each macro-particle corresponds to a cloud of physical particles with realistic properties. The motion of these macro-particles is governed by electromagnetic forces, while the electromagnetic fields are advanced using Maxwell's equations together with the charge and current densities derived from the particle distribution. Vlasov models, in contrast, evolve the full phase-space distribution function directly in time while simultaneously solving Maxwell's equations. Because fully kinetic models include electron-scale physics, the smallest electron spatial and temporal scales dictate the required grid resolution and time step. This results in high computational costs, making it infeasible with current computing capabilities to simulate the Earth–solar-wind interaction at realistic scales using fully kinetic approaches.

6.1.4 *Hybrid-kinetic models*

A compromise between MHD models and fully kinetic models are hybrid models. In these models, ion dynamics are treated kinetically, while electrons are modeled as a massless, charge-neutralizing fluid. Hybrid models therefore capture ion-scale kinetic physics while still evolving the electromagnetic fields self-consistently. Their computational cost lies between that of MHD and fully kinetic simulations, and recent increases in computing power have made it possible to model Earth's plasma environment in full 3D using hybrid-PIC approaches (Fatemi et al., 2024b; Guo et al., 2025) as well as hybrid-Vlasov models (Von Alfthan et al., 2014). Since the formation of jets is linked to ion-kinetics in the foreshock and bow shock regions, MHD models cannot generate jets self-consistently, but hybrid models are required at a minimum. In

the following section, the hybrid model Amitis (Fatemi et al., 2017) is introduced which is used in Paper II and III to investigate magnetosheath jets through simulations.

6.2 THE HYBRID MODEL AMITIS

Amitis (Fatemi et al., 2017) is a GPU-based, hybrid kinetic plasma model. The upgraded version of the model can run on multiple GPUs in parallel (Fatemi et al., 2022) and has been successfully applied to model the near-Earth plasma environment (Fatemi et al., 2024b). In Amitis, ions are modeled as macro-particles while electrons are a massless, charge-neutralizing fluid. The model is grid-based and three dimensional in both configuration space and velocity. The model is also time-dependent, which means the input parameters can be changed at the inflow boundary representing a change in the solar wind.

6.2.1 *Model Equations*

The following equations and approximations apply to hybrid-PIC models in general (Ledvina et al., 2008), but we in particular focus on the implementation in Amitis (Fatemi et al., 2017).

The first assumption is charge neutrality which is valid on scales larger than the Debye length λ_D. This implies a minimum size for the simulation grid which needs to be larger than λ_D. The total charge density ρ fulfills

$$\rho = \rho_e + \rho_I = 0, \tag{6.1}$$

where ρ_e is the electron charge density, and ρ_I the total ion charge density defined as

$$\rho_I = \sum_{i=1}^{N} \rho_i, \tag{6.2}$$

where ρ_i denotes the charge density for an individual ion species and N is the number of ion species.

Amitis uses the Darwin approximation which means that the transverse displacement current is neglected in Ampere's law, Equation (2.17), so it reduces to

$$\mathbf{J} = \frac{\nabla \times \mathbf{B}}{\mu_0}, \tag{6.3}$$

where $\mathbf{B}$ is the magnetic field, $\mathbf{J}$ the current density, and μ_0 the vacuum permeability. The electron current density $\mathbf{J}_e$ can be calculated using

$$\mathbf{J}_e = \mathbf{J} - \mathbf{J}_I, \tag{6.4}$$

where J_I is the total ion current densities which fulfills

$$\mathbf{J}_I = \sum_{i=1}^{N} \mathbf{j}_i = \sum_{i=1}^{N} q_i n_i \boldsymbol{v}_i. \tag{6.5}$$

$\mathbf{J}_I$ can be calculated from the particle distribution in the model itself. The Darwin approximation removes relativistic phenomena and light waves from the simulation.

The momentum equation for massless ($m_e = 0$) electrons is used to get an expression for Ohm's law (Equation (2.13) without the $\frac{\partial \mathbf{j}}{\partial t}$ term)

$$\mathbf{E} = -\frac{\mathbf{J}_I \times \mathbf{B}}{\rho_I} + \left(\frac{\nabla \times \mathbf{B}}{\mu_0}\right) \times \frac{\mathbf{B}}{\rho_I} - \frac{\nabla \cdot \overline{\mathbf{P}}_e}{\rho_I} + \frac{\eta}{\mu_0} \nabla \times \mathbf{B}, \tag{6.6}$$

where η is the resistivity and $\overline{\mathbf{P}}_e$ is the electron pressure tensor.

In Amitis the electron pressure $P_e = n_e k_b T_e$ is assumed to be adiabatic, the electron pressure is therefore related to the charge density by $P_e \sim |\rho_e|^\gamma$ with γ the adiabatic index.

The magnetic field is advanced in time using Faraday's law

$$\frac{\partial \mathbf{B}}{\partial t} = -\nabla \times \mathbf{E}, \tag{6.7}$$

with $\mathbf{E}$ obtained from Equation (6.6).

The position and velocities of macro-particles (representing ions) with charge q_i and mass m_i are updated using the equation of motions

$$\frac{d\mathbf{r}_i}{dt} = \boldsymbol{v}_i, \tag{6.8}$$

$$\frac{d\boldsymbol{v}_i}{dt} = \frac{q_i}{m_i} \left(\mathbf{E} + \boldsymbol{v}_i \times \mathbf{B}\right). \tag{6.9}$$

The model does explicitly solve for the electron fluid, but the assumption of massless electrons enters the model equation through momentum equation for massless electrons that is used to get an expression for the electric field, Equation (6.6).

6.2.2 *Simulation of near-Earth plasma environment*

This section describes the simulation set up that was used for Paper II and Paper III. More details on the Amitis simulation applied to the Earth plasma environment can be found in Fatemi et al. (2024b).

Coordinate system

Generally, different coordinate systems can be used in hybrid simulations, the Amitis models employs a cartesian coordinate system with Earth at its origin. The $+x$-axis points towards the Sun, the $+z$-axis points toward the northern magnetic dipole, and $+y$-axis completes the right-handed coordinate system. The coordinate system is indicated in the bottom right corner of Figure 6.1.

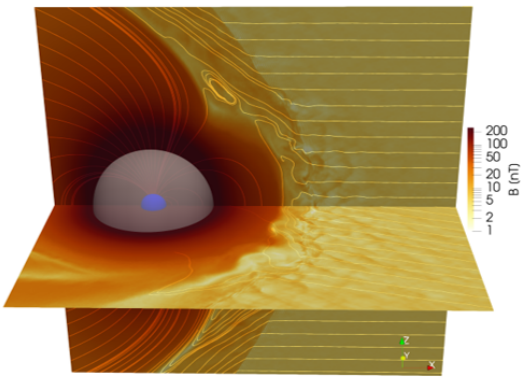

Figure 6.1: Snapshot showing the magnetic field from an Amitis simulation run with an almost radial IMF. The streamlines represent magnetic field lines projected onto the xy- and xz-planes, respectively. The white sphere at the center represents the inner conducting boundary, while the smaller blue sphere represents Earth. This snapshot does not show the entire simulation domain, but rather a close-up of the near-Earth plasma environment. Add coordinate grid?

Simulation domain and grid size

The dimensions of the simulations domain vary slightly between different simulation runs. Check the exact simulation domains and put them in a table. Generally, the inflow boundary is at $x \approx +53\,R_E$, where $1\,R_E = 6371\,\text{km}$ is the radius of Earth. At the inflow boundary macroparticles are continuously injected into the simulation domain. The outflow boundary at $x \approx -20\,R_E$ is a perfect plasma absorber where all particles are removed. The boundaries at $(y, z) \approx \pm 55\,R_E$ are periodic boundaries such that the electromagnetic fields and particles are moved from one side to the other side of the simulation domain. In addition, the inner boundary of the magnetosphere is modeled as a conducting sphere with a radius of 30000 km ($\approx 4.7\,R_E$) centered at the origin. This inner boundary is also a perfect plasma observer where particles are removed from the simulation domain. To lower the computational cost of simulation runs, the inner boundary is set larger than the actual Earth radius. Figure 6.1 shows the size of the inner conducting boundary (white, transparent sphere in the center) in comparison to Earth's size (smaller blue sphere in the center). Since the model is not used to study the inner magnetosphere, but the main focus is the magnetosheath, a model for the atmosphere and ionosphere are also not included in the simulation.

The simulation domain is discretized using a Cartesian grid with cubic cells of size 500 km ($\approx 0.78\,R_E$).

6.2.2.1 *Simulation design*

The properties of the electromagnetic field and the macro-particles at the inflow boundary represent the solar wind conditions. In the simulation runs used in Paper II and III, only solar wind protons were modeled, neglecting heavier solar wind ions for simplicity since the majority of solar wind ions are protons (Russell, Luhmann et al., 2016).

We aimed to model 'typical' solar wind conditions near Earth (Ma et al., 2020) setting the solar wind speed to 400 km/s, density to $7\,\mathrm{cm}^{-3}$, and the temperature to 10 eV in each direction. The magnetic field magnitude is to 5 nT. The direction of the IMF was varied for different simulation runs. We used runs where the IMF was almost radial, forming a 15° angle with the Sun-Earth line, and runs with the IMF perpendicular to the Sun-Earth line. This allows us to study the interaction with and without a foreshock in the foreshock in the subsolar region.

To model the near-Earth plasma environment a realistic scales, the Earth's magnetic field needs to represented at realistic scales. Therefore, a dipole magnetic moment $M = 8.22 \times 10^{22}\,\mathrm{Am}^2$ (Walt, 1994) was used in the simulation runs. Higher order moments of the Earth's magnetic field are not included.

Time step size

The maximum time step between two simulation time steps is determined by the Courant-Friedrichs-Lewy (CFL) condition (Courant et al., 1928). For eq. (6.7) without the Ohmic term ($\eta\nabla \times \mathbf{B}/\mu_0$) the CFL condition is

$$\Delta t < \frac{\omega_g}{\sqrt{3}\pi}\left(\frac{\Delta h}{v_A}\right)^2, \tag{6.10}$$

where ω_g is the gyro frequency, and v_A is the Alfvén speed, Δh is the length of grid cell. The CFL condition needs to be met to ensure accurate propagation of the electromagnetic fields according the Faraday's and Ohm's law. Including the resistive term in the electric field (eq. (6.6)) would require a much smaller time steps which is computationally expensive. To avoid using smaller time steps, the Amitis model uses an explicit-implicit scheme, where the electric field without the Ohmic term is solved explicitly and the Ohmic term is solved implicitly. Explicit schemes calculate the state of the simulation of a later time only by using the current state. While implicit schemes solve an equation from the current and future states [1]. The implicit scheme allows for larger time steps for the Ohmic term and the simulation time steps is therefore determined by the CFL condition (eq. (6.10)) for the explicit scheme.

1 Implicit schemes are more difficult to implement and computationally more expensive. Due to the simplicity of explicit schemes, they are easier to implement and therefore commonly used.

Remarks on the ion scale length

Modeling the interaction between the solar wind and Earth's magnetic field using a hybrid model is computationally expensive, even when employing GPUs. Therefore, hybrid simulations of the near-Earth plasma environment have often used a reduced Earth magnetic dipole moment or fewer spatial dimensions (e.g., Omelchenko et al., 2021; Palmroth et al., 2020). A reduced dipole moment results in a scaled near Earth plasma environment, such that the relative size of different phenomena are not realistic, for example the size of jets is different relative to the size of the magnetosheath. Fewer spatial dimension comes at the cost of not being able to simulate the 3D structure of magnetosheath jets which has been shown to be highly interconnected and dynamic (Fatemi et al., 2024b; Guo et al., 2025). Alternatively, a larger simulation cell size can be used, as was done in the Amitis simulation run described in Papers II and III. In general, hybrid models require the simulation grid size Δh to be at least an order of magnitude larger than the electron inertial length $\delta_e = c/\omega_{pe}$, where c is the speed of light and ω_{pe} is the electron plasma frequency (Ledvina et al., 2008). Using the ratio $\delta_i/\delta_e = \sqrt{m_i/m_e} \approx 43$, this implies that the grid size should satisfy $\Delta L > 10\,\delta_e = 10\,\delta_i/43 \approx 0.25\,\delta_i$.

However, in our simulation runs we instead use $\Delta L = 500\,\mathrm{km} \approx 5.8\,\delta_i$. This choice is motivated by the findings of Tóth et al. (2017), who showed that as long as the global scales and the ion inertial scale remain well separated in hybrid simulations, the global solution is not sensitive to the exact value of the ion inertial length. In particular, ion-inertial-scale dynamics are shifted to larger spatial scales, while intermediate-scale features, those several ion inertial lengths across, still grow in a self-similar manner. Since our interest lies primarily in jets which typically have scale sizes larger than $0.1\,R_E$, we do not expect any issues arising from the increased cell size. Furthermore, we focus on global dynamics arising from magnetosheath jets rather than the internal structure of jets.

Simulation output

While the simulation advances with a time step of 8 ms, the output is written only every few seconds to reduce disk space usage. The simulation output consists of grid-defined quantities as well as positions and velocities of macro-particles. The grid-defined quantities include the electric field, magnetic field, ion current density, and charge density. From these, additional parameters such as number density and bulk velocity can be derived. Figure 6.2 shows the magnetic field, plasma density, bulk speed, and current density for a simulation run with a quasi-radial IMF at 18:32.

The plasma temperature or thermal velocity is not part of the simulation output, as it is not included in the model equations. In Paper II,

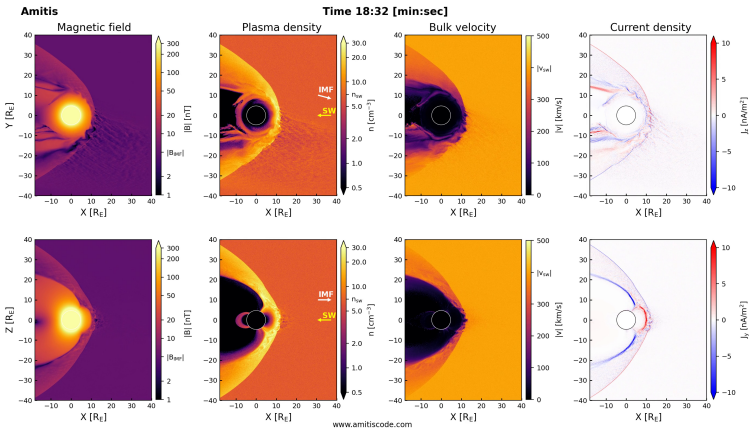

Figure 6.2: Example output from Amitis simulation at time step 18:32 for an simulation run with quasi-radial IMF. The magnetic field strength $|B|$, plasma density n, bulk speed $|v|$, and components of the current density j are shown in the $z = 0$-plane (upper row) and $y = 0$-plane (lower row). Make plot with larger fontsize? Write bulk speed instead of bulk velocity?

we investigated the energy input of jets into the magnetosheath. Estimating the thermal energy requires a temperature or thermal velocity, so we used the particle energy

$$\begin{aligned} E_p &= \frac{1}{2} m \sum_{i=0}^{N} v_i^2 \\ &= \frac{1}{2} m \sum_{i=0}^{N} (\langle v \rangle - \langle v \rangle + v_i)^2 \\ &= \frac{1}{2} m \sum_{i=0}^{N} \langle v \rangle^2 + \frac{1}{2} m \sum_{i=0}^{N} (v_i - \langle v \rangle)^2 \\ &= E_{kin} + E_{th}, \end{aligned}$$

where N is the number of particles in a volume, v_i is the velocity of the i-th particle, and $\langle v \rangle = \frac{1}{N} \sum_i v_i$ is the bulk velocity. This calculation requires access to the individual particle velocities rather than grid-based quantities. Since the Amitis model uses an interpolation scheme to assign a fraction of a macro particles charge to its neighboring cells, we recalculated the bulk velocities and densities directly from the particle positions and only assigned each macro-particle to its nearest simulation center.

7 SUMMARY OF PAPERS

In this section we provide a summary of the appended papers.

7.1 PAPER I: WAVES IN MAGNETOSHEATH JETS—CLASSIFICATION AND THE SEARCH FOR GENERATION MECHANISMS USING MMS BURST MODE DATA

Paper I (Krämer et al., 2023) investigates wave activity inside and around three magnetosheath jets using MMS burst-mode data. The use of burst mode data allows us to resolve higher-frequency wave modes compared to previous studies of jet-associated wave activity (Gunell et al., 2014; Karlsson et al., 2018). We identify several wave types: 1 Hz waves, whistler waves, electron acoustic waves, waves near the lower hybrid frequency, electrostatic solitary waves, and 0.2 Hz waves. Electron acoustic waves contribute significantly to broadband electrostatic noise, whereas electrostatic solitary waves play only a minor role. Our observations of whistler waves, lower hybrid waves, and 0.2 Hz waves are consistent with previous reports of waves in jets (Gunell et al., 2014; Karlsson et al., 2018).

Electrostatic solitary waves, electron acoustic waves, and whistler-mode waves exhibit properties expected from linear theory in a homogeneous plasma. In contrast, the 0.2 Hz, 1 Hz, and lower hybrid waves deviate from these assumptions, showing characteristics of multiple different wave modes.

Finally, we examine possible generation mechanisms. The 1 Hz waves likely arise from magnetic field and density gradients. Whistler waves appear to be driven by butterfly-shaped pitch-angle distributions, while electron acoustic waves are associated with cold electron populations. For the remaining described waves, we could not identify the source due to instrumental limitations.

Contributions: I performed the data analysis of the MMS data, and wrote the paper with the comments and edits by the co-authors.

7.2 PAPER II: ON THE KINETIC ENERGY INPUT OF MAGNETOSHEATH JETS INTO THE MAGNETOSHEATH

Paper II (Krämer, Fatemi et al., 2025) investigates the energy exchange between jets and the surrounding magnetosheath plasma. For this analysis, we employ the 3D hybrid-kinetic model Amitis at realistic scales. Using the simulation, we define a volume within the magnetosheath with a well-defined surface normal vectors. Our study focuses on two

simulation runs: one with an almost radial IMF and another with the IMF oriented along the z-axis.

In the radial IMF simulation run, jets occupy up to 21% of the volume and account for nearly half of the kinetic energy in the subsolar magnetosheath. This indicates that jets carry a significant amount of mass, energy, and momentum in the quasi-parallel magnetosheath. In contrast, in the simulation run where the IMF is aligned along z, their contribution becomes negligible, and jets are confined to regions near the bow shock. Consequently, jets play a minor role in the quasi-perpendicular magnetosheath.

We further compute particle and energy fluxes across the surface of the selected volume. Our results show that jets partly degenerate as they propagate through the magnetosheath. They also transport excess energy into the magnetosheath, primarily contributing to plasma heating in the quasi-radial IMF simulation run. Finally, we discuss the influence of jet detection criteria: relying on a single velocity component rather than total speed skews the energy input due to the deflection of jets around the planet.

Contributions: I organized the study, performed the data analysis, and wrote the paper with the comments and edits by the co-authors.

7.3 PAPER III: MAGNETOSHEATH JET INTERACTION WITH THE MAGNETOPAUSE: RESULTS FROM THE 3D HYBRID-KINETIC SIMULATION AMITIS

Paper III (Citation (hopefully accepted)!) investigates the interaction between magnetosheath jets and the magnetopause using the global three-dimensional hybrid kinetic simulation Amitis. Because the position of the magnetopause is determined by pressure balance between the solar wind dynamic pressure and Earth's magnetic field, transient pressure enhancements in the magnetosheath can cause localized magnetopause displacements. Spacecraft observations have shown such transient magnetopause motions associated with jet impacts, however, resolving the full spatial and temporal interaction is challenging due to the limited number of simultaneous observation points. To overcome these limitations, we employ a global 3D simulation to examine the spatial and temporal evolution of jets interacting with the magnetopause.

Our results show that jets downstream of the quasi-parallel bow shock can excite magnetopause surface waves and continuously drive their propagation, see also figure 7.1. An interesting aspect of this interaction is that the bulk velocity of ions within a jet differs from the apparent motion of the jet itself. We interpret this behavior as evidence for continuous jet generation at the bow shock, potentially driven by foreshock compressive structures. In addition, we find indications that jets can potentially trigger the development of Kelvin-Helmholtz vortices at the magnetopause.

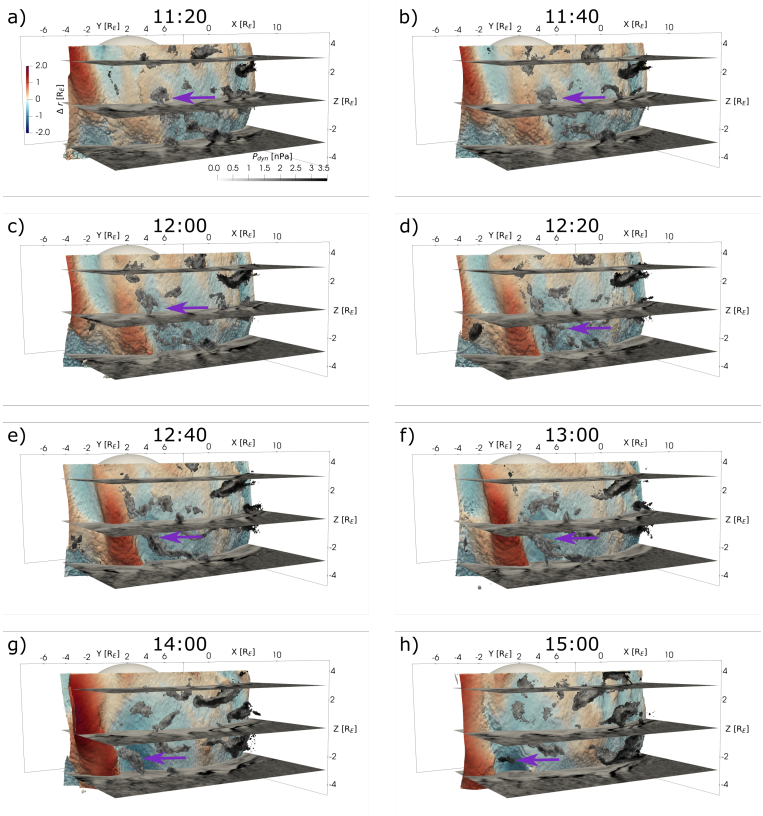

Figure 7.1: Crop figure and only show part? Add citation. Results from the Amitis simulation showing the interaction between jets and the magnetopause at different time steps indicated at the top each panel.

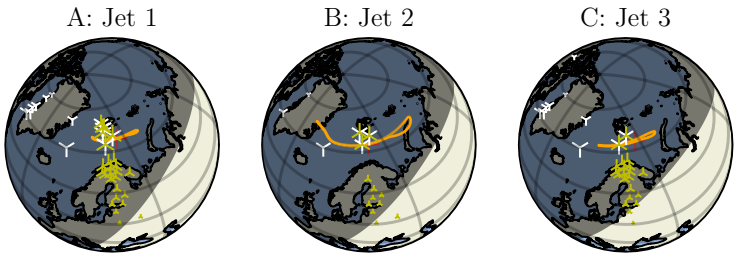

Figure 7.2: Estimated footpoint of the jet impacts at the magnetopause as red cross. Magnetometer stations that were affected by the jet impact indicated by white and yellow markers. Figure reproduced from Krämer, Hamrin, Gunell et al. (2025), licensed under CC BY 4.0.

7.4 PAPER IV: MAGNETOSHEATH JET-TRIGGERED ULF WAVES: ENERGY DEPOSITION IN THE IONOSPHERE

Paper IV (Krämer, Hamrin, Gunell et al., 2025) presents a case study in which we investigate energy deposition in the ionosphere caused by jet-triggered ULF waves. When jets impact the magnetopause, they can locally excite ULF waves that couple to field-aligned Alfvén waves propagating into the ionosphere, thereby transporting energy downward. In the ionosphere, these waves produce localized magnetic field disturbances that can be detected by ground-based magnetometers, see figure 7.2. We estimated the ionospheric energy deposition for two jets observed by the MMS spacecraft on 2016-01-07.

To estimate the energy deposition in the ionosphere, we assumed that the incoming Poynting flux is dissipated through Joule heating. By combining electric field measurements from SuperDARN with estimates of the height-integrated Pedersen conductivity obtained from the EISCAT radar, we approximated the average Joule heating rate to 0.38 mW/m for the two jet-events. This estimate is comparable to the Joule heating rate of field line resonances. Using ground-based magnetometer data to estimated the affected area, we concluded that the average energy input per jet impact was $9 \cdot 10^{10}$ J. Even under favorable solar wind conditions, when several jets can impact the magnetopause per hour, we find that the total energy deposition in the ionosphere due to jets is small compared to other magnetospheric processes, primarily because of the limited ground area affected.

Contribution: I organized the study, performed the data analysis, and wrote the paper with the comments and edits by the co-authors.

7.5 PAPER V: JETS DOWNSTREAM OF THE MARTIAN BOW SHOCK – OCCURRENCE IN THE 2014–2024 PERIOD

Paper V (Mohammed-Amin et al., 2025) presents the first statistical study of jets downstream of the Martian bow shock. Our jet database, compiled from ten years of MAVEN observations, contains a total of 82645 events. On average, the dynamic pressure increases by a factor of 2.34. We find that most jets are driven by both density and velocity enhancements, with the density contribution being dominant. Similar to jets at Earth, the majority of Martian magnetosheath jets are located near the bow shock and tend to be colder and more isotropic than the surrounding plasma. Additionally, these jets often exhibit an increase in magnetic field strength.

However, notable differences exist compared to jets in the terrestrial magnetosheath. Jets in the Martian magnetosheath are more strongly deflected relative to the ambient plasma and are generally smaller, with a median scale size of $0.67\,R_M$. Nevertheless, when compared to the overall size of the Martian magnetosphere, these jets are relatively larger than their terrestrial counterparts.

Contributions: I wrote half the paper and contributed to the planning of the study.

7.6 PAPER VI: MAGNETOSPHERIC VENUS SPACE EXPLORERS (MVSE) MISSION: A PROPOSAL FOR UNDERSTANDING THE DYNAMICS OF INDUCED MAGNETOSPHERES.

Paper VI (Albers et al., 2024) presents the *Magnetospheric Venus Space Explorers (MVSE)* mission concept, which aims to investigate the dynamics of induced magnetospheres. Induced magnetospheres develop around unmagnetized bodies with atmospheres. Those induced magnetospheres are highly variable plasma environments whose state strongly depends on solar wind conditions. Previous and ongoing missions to bodies with induced magnetospheres have largely relied on single-point measurement, making it difficult to establish a direct casual link between varying solar wind conditions and the magnetospheric response. In particular also variations due to extreme solar events. The magnetospheric system of Venus is the most prominent example of an induced magnetosphere in the solar system and is therefore an ideal target for studying the spatial and temporal variability of a Venusian plasma environment.

We present the mission's scientific questions and the corresponding scientific requirements, from which the mission requirements are derived. The proposed scientific payload enables measurements of magnetic and electric fields as well as ion and electron distributions. We further describe the mission timeline and the orbital configuration of each spacecraft. The mission comprises three identical scientific spacecraft and one transfer module, the latter also serves as the communic-

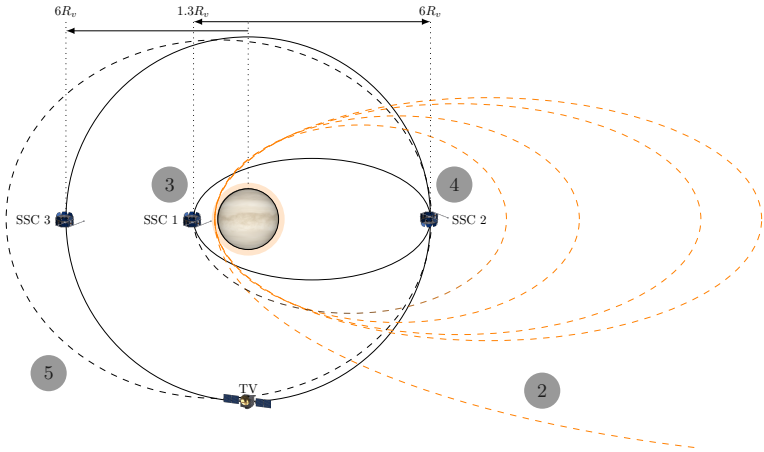

Figure 7.3: Orbits for the three science spacecraft and communication vehicle for the proposed MVSE mission. Reproduced from Albers et al. (2024), licensed under CC BY 4.0.

ations relay. The orbits are designed such that one spacecraft monitors the upstream solar wind while two spacecraft perform in situ measurements within the Venusian plasma environment. The proposed orbits for the spacecraft are depicted in figure 7.3. We also outline the spacecraft design driven by the mass, power, and communication budgets.

This mission concept was developed during the Alpbach Summer School 2022 by Team Yellow and was further refined during the Post Alpbach Summer School event.

Contributions: As a part of Team Yellow during the Alpbach Summer School 2022, I helped to develop the mission concept, in particular by contributing the the scientific goals and requirements of the mission. During the Post Alpbach Summer School event I was responsible for the scientific payload. I also contributed by writing and editing Sections 1-3 of the paper.

8

OUTLOOK

This thesis has shown that magnetosheath jets evolve significantly as they propagate, act as drivers of magnetopause dynamics, and occur across different planetary environments.

We investigated the propagation of magnetosheath jets from two complementary perspectives: global three-dimensional simulations and local, high time-resolution spacecraft observations. The global hybrid-kinetic simulations show that jets gradually disintegrate as they traverse the magnetosheath, indicating that their excess kinetic energy is converted into thermal energy. However, these simulations do not directly reveal the mechanisms responsible for this energy conversion. To gain insight into the underlying processes, we turn to spacecraft observations. These observations reveal enhanced wave activity both within and the vicinity of jets. In particular, low-frequency electromagnetic waves may play an important role in redistributing jet energy, potentially radiating away excess kinetic energy on timescales comparable to the jet transit time through the magnetosheath (Karlsson et al., 2018). However, it remains unclear whether and how these waves contribute to plasma heating, and which specific instabilities are responsible for their generation. Identifying the source of these waves is challenging because the plasma within and around jets is far from equilibrium, for example density gradients (Krämer et al., 2023), velocity shears (Plaschke and Hietala, 2018), or non-Maxwellian velocity distribution functions (e.g. Blanco-Cano et al., 2020; Raptis, Karlsson, Vaivads, Lindberg et al., 2022; Roberts et al., 2025) can be present. While multi-spacecraft observations, such as those from the MMS mission (Burch et al., 2016), enable the estimation of local gradients, they are inherently limited by spacecraft separations that are small compared to typical jet scales assuming linearity and stationary processes. However, jets are non-stationary and while their volume is closer to fluid scales, energy conversion are caused by wave-particle interaction at ion or electron scales. To overcome this limitations the mission concept Plasma Observatory (Retinò et al., 2022) aims to probe plasma processes on scales comparable to those of jets and simultaneous probing smaller scales. Beyond identifying specific wave modes, a more general approach to quantifying energy conversion is provided by the pressure–strain method, which directly quantifies the transfer between bulk flow energy and thermal energy. This method assess whether heating arises primarily from plasma compression or from incompressible processes. Applying such method to both spacecraft observations and global simulations can connect local dissipation mechanisms with the large-scale evolution of jets. Overall, jet

evolution connects to the broader question of how energy injected at collisionless shocks is redistributed and dissipated in space plasmas.

As jets move across the magnetopause they disintegrate, yet some jets still reach the boundary. Upon impact, these jets can locally displace the magnetopause due to their enhanced dynamic pressure on the magnetosheath side. However, our results suggest that the jet–magnetopause interaction is not typically governed by isolated, "bullet-like" impacts. Instead, it is dominated by continuous jet formation at the bow shock, which drives a sustained perturbation of the magnetopause. Through this interaction, jets can also generate ultra-low frequency (ULF) waves, in particular Pc5 waves, within the magnetosphere (Norenius et al., 2021; Wang et al., 2022). These waves are known to transport energy and momentum through the magnetospheric system and input energy into the ionosphere. Despite the large amplitude of jet-triggered waves, our results indicate that jet-driven Pc5 waves are not a dominant source of energy input into the ionosphere. However, their impact cannot be fully assessed by ionospheric effects alone. Pc5 waves play an important role within the magnetosphere itself, for example by accelerating electrons through drift resonance (Koskinen et al., 2022). This raises the question of whether jet-driven disturbances at the magnetopause can propagate to sufficient amplitudes deeper within the magnetosphere to influence radiation belt dynamics and modulate particle fluxes. Addressing this question requires coordinated observations between spacecraft in the magnetosheath and those probing the inner magnetosphere, such as the Van Allen Probes (Mauk et al., 2013) and the Arase satellite (Miyoshi et al., 2018). Furthermore, our results suggest that magnetosheath jets should be viewed not only as localized pressure enhancements but as a driver of large-scale boundary dynamics. Understanding how such boundary-driven disturbances propagate and interact with internal magnetospheric processes remains a key challenge for quantifying their role in the global system. In summary, this highlights the role of localized structures in mediating the coupling between the solar wind and the magnetosphere.

Finally, extending the study of magnetosheath jets beyond Earth to other plasma environments contributes to a more universal understanding of their formation and effects. Although jets have only recently been investigated in other plasma environments (Krämer et al., 2024), they provide a valuable insights of bow shock dynamics across different environments. Observational datasets are limited, and instrumental limitations pose challenges for jet detection. However, upcoming missions such as BepiColombo at Mercury (Benkhoff et al., 2021) may provide new opportunities for observational validation. In parallel, numerical models such as Amitis, which have already been applied to Mercury, Mars, and cometary environments (e.g. Fatemi et al., 2020; Gunell et al., 2024; Moeslinger et al., 2024; Moeslinger et al., 2025; Nesbit-Östman, 2025; Shi et al., 2025; Wang et al., 2024), can be extended to investigate

jet formation and evolution in different environments. Such comparative studies may reveal how jets form across different planetary systems and interact with induced magnetospheres and magnetospheres of different scale size and may therefore provide insight into universal processes governing collisionless plasma interactions.

Taken together, these directions highlight the importance of combining multi-scale observations, global simulations, and cross-environment comparisons to achieve a comprehensive understanding of magnetosheath jets and their role in plasma systems. Ultimately, magnetosheath jets contribute to the transfer and dissipation of energy across scales and plasma boundaries, a fundamental problem in space and astrophysical plasmas.

BIBLIOGRAPHY

Albers, Roland, Henrik Andrews, Gabriele Boccacci, Vasco DC Pires, Sunny Laddha, Ville Lundén, Nadim Maraqten, João Matias, Eva Krämer, Leonard Schulz et al. (2024). "Magnetospheric Venus Space Explorers (MVSE) mission: A proposal for understanding the dynamics of induced magnetospheres". In: *Acta Astronautica* 221, pp. 194–205.

Angelopoulos, V. (2008). "The THEMIS Mission". In: *Space Science Reviews* 141.1–4, pp. 5–34. ISSN: 0038-6308, 1572-9672. DOI: 10.1007/s11214-008-9336-1.

Angelopoulos, V. (2011). "The ARTEMIS Mission". In: *Space Science Reviews* 165.1–4, pp. 3–25. ISSN: 0038-6308, 1572-9672. DOI: 10.1007/s11214-010-9687-2.

Archer, M. O. and T. S. Horbury (2013). "Magnetosheath Dynamic Pressure Enhancements: Occurrence and Typical Properties". In: *Annales Geophysicae* 31.2, pp. 319–331. ISSN: 1432-0576. DOI: 10.5194/angeo-31-319-2013.

Archer, M. O., T. S. Horbury and J. P. Eastwood (2012). "Magnetosheath Pressure Pulses: Generation Downstream of the Bow Shock from Solar Wind Discontinuities: MAGNETOSHEATH PRESSURE PULSES". In: *Journal of Geophysical Research: Space Physics* 117.A5, n/a–n/a. ISSN: 01480227. DOI: 10.1029/2011JA017468.

Archer, M. O., D. L. Turner, J. P. Eastwood, S. J. Schwartz and T. S. Horbury (2015). "Global Impacts of a Foreshock Bubble: Magnetosheath, Magnetopause and Ground-Based Observations". In: *Planetary and Space Science* 106, pp. 56–66. ISSN: 0032-0633. DOI: 10.1016/j.pss.2014.11.026.

Archer, Martin, Timothy S. Horbury, J. P. Eastwood, Jonathan Eastwood, James M. Weygand and Tim K. Yeoman (2013). "Magnetospheric Response to Magnetosheath Pressure Pulses: A Low Pass Filter Effect". In: *Journal of Geophysical Research* 118.9, pp. 5454–5466. DOI: 10.1002/jgra.50519.

Auster, H. U. et al. (2008). "The THEMIS Fluxgate Magnetometer". In: *Space Science Reviews* 141.1, pp. 235–264. ISSN: 1572-9672. DOI: 10.1007/s11214-008-9365-9.

Baumjohann, Wolfgang and Rudolf A Treumann (2012). *Basic space plasma physics*. World Scientific.

Belmont, Gerard and Gerard Chanteur (1989). "Advances in Magnetopause Kelvin-He1mholtz Instability Studies". In: *Physica Scripta* 40.1, pp. 124–128.

Benkhoff, J. et al. (2021). "BepiColombo - Mission Overview and Science Goals". In: *Space Science Reviews* 217.8, p. 90. ISSN: 1572-9672. DOI: 10.1007/s11214-021-00861-4.

Bertucci, C., F. Duru, N. Edberg, M. Fraenz, C. Martinecz, K. Szego and O. Vaisberg (2011). "The Induced Magnetospheres of Mars, Venus, and Titan". In: *Space Science Reviews* 162.1, pp. 113–171. ISSN: 1572-9672. DOI: 10.1007/s11214-011-9845-1.

Blanco-Cano, X., L. Preisser, P. Kajdič and D. Rojas-Castillo (2020). "Magnetosheath Microstructure: Mirror Mode Waves and Jets during Southward IP Magnetic Field". In: *Journal of Geophysical Research: Space Physics* 125.9. ISSN: 2169-9380, 2169-9402. DOI: 10.1029/2020JA027940.

Brain, D A, F Bagenal and M H Acu (2003). "Martian Magnetic Morphology: Contributions from the Solar Wind and Crust". In: *Journal of Geophysical Research: Space Physics* 108.A12. DOI: 10.1029/2002JA009482.

Büchner, Jörg (2005). "Vlasov-code simulation". In: *Proceedings of ISSS*. Vol. 7, pp. 26–31.

Burch, J. L., T. E. Moore, R. B. Torbert and B. L. Giles (2016). "Magnetospheric Multiscale Overview and Science Objectives". In: *Space Science Reviews* 199.1, pp. 5–21. ISSN: 1572-9672. DOI: 10.1007/s11214-015-0164-9.

Case, NA and JA Wild (2012). "A statistical comparison of solar wind propagation delays derived from multispacecraft techniques". In: *Journal of Geophysical Research: Space Physics* 117.A2.

Connerney, J. E. P., J. Espley, P. Lawton, S. Murphy, J. Odom, R. Oliversen and D. Sheppard (2015). "The MAVEN Magnetic Field Investigation". In: *Space Science Reviews* 195.1–4, pp. 257–291. ISSN: 0038-6308, 1572-9672. DOI: 10.1007/s11214-015-0169-4.

Courant, Richard, Kurt Friedrichs and Hans Lewy (1928). "Über die partiellen Differenzengleichungen der mathematischen Physik". In: *Mathematische annalen* 100.1, pp. 32–74.

Cravens, Thomas E. (2004). *Physics of Solar System Plasmas*.

Dmitriev, A. V. and A. V. Suvorova (2012). "Traveling Magnetopause Distortion Related to a Large-Scale Magnetosheath Plasma Jet: THEMIS and Ground-Based Observations". In: *Journal of Geophysical Research: Space Physics* 117.A8. ISSN: 2156-2202. DOI: 10.1029/2011JA016861.

Eastwood, JP, EA Lucek, C Mazelle, K Meziane, Y Narita, J Pickett and RA Treumann (2005). "The foreshock". In: *Space Science Reviews* 118.1, pp. 41–94. DOI: 10.1007/s11214-005-3824-3.

Edberg, N. J. T., M. Lester, S. W. H. Cowley and A. I. Eriksson (2008). "Statistical Analysis of the Location of the Martian Magnetic Pileup Boundary and Bow Shock and the Influence of Crustal Magnetic Fields". In: *Journal of Geophysical Research: Space Physics* 113.A8. ISSN: 2156-2202. DOI: 10.1029/2008JA013096.

Ergun, R. E. et al. (2016). "The Axial Double Probe and Fields Signal Processing for the MMS Mission". In: *Space Science Reviews* 199.1, pp. 167–188. ISSN: 1572-9672. DOI: 10.1007/s11214-014-0115-x.

Escoubet, C. Philippe et al. (2020). "Cluster and MMS Simultaneous Observations of Magnetosheath High Speed Jets and Their Impact on the Magnetopause". In: *Frontiers in Astronomy and Space Sciences* 6, p. 78. ISSN: 2296-987X. DOI: 10.3389/fspas.2019.00078.

Fairfield, Donald H. (1971). "Average and Unusual Locations of the Earth's Magnetopause and Bow Shock". In: *Journal of Geophysical Research (1896-1977)* 76.28, pp. 6700–6716. ISSN: 2156-2202. DOI: 10.1029/JA076i028p06700.

Fatemi, S, M Hamrin, E Krämer, H Gunell, G Nordin, T Karlsson and O Goncharov (2024a). "Unveiling the 3D Structure of Magnetosheath Jets". In: *Monthly Notices of the Royal Astronomical Society* 531.4, pp. 4692–4713. ISSN: 0035-8711, 1365-2966. DOI: 10.1093/mnras/stae1456.

Fatemi, S, M Hamrin, E Krämer, H Gunell, G Nordin, T Karlsson and O Goncharov (2024b). "Unveiling the 3D Structure of Magnetosheath Jets". In: *Monthly Notices of the Royal Astronomical Society* 531.4, pp. 4692–4713. ISSN: 0035-8711, 1365-2966. DOI: 10.1093/mnras/stae1456.

Fatemi, S., A. R. Poppe and S. Barabash (2020). "Hybrid Simulations of Solar Wind Proton Precipitation to the Surface of Mercury". In: *Journal of Geophysical Research: Space Physics* 125.4, e2019JA027706. ISSN: 2169-9402. DOI: 10.1029/2019JA027706.

Fatemi, S., A. R. Poppe, A. Vorburger, J. Lindkvist and M. Hamrin (2022). "Ion Dynamics at the Magnetopause of Ganymede". In: *Journal of Geophysical Research: Space Physics* 127.1, e2021JA029863. ISSN: 2169-9402. DOI: 10.1029/2021JA029863.

Fatemi, Shahab, Andrew R. Poppe, Gregory T. Delory and William M. Farrell (2017). "AMITIS: A 3D GPU-Based Hybrid-PIC Model for Space and Plasma Physics". In: *Journal of Physics: Conference Series* 837, p. 012017. ISSN: 1742-6588, 1742-6596. DOI: 10.1088/1742-6596/837/1/012017.

Futaana, Yoshifumi, Gabriella Stenberg Wieser, Stas Barabash and Janet G. Luhmann (2017). "Solar Wind Interaction and Impact on the Venus Atmosphere". In: *Space Science Reviews* 212.3–4, pp. 1453–1509. ISSN: 0038-6308, 1572-9672. DOI: 10.1007/s11214-017-0362-8.

Gjerloev, J. W. (2009). "A Global Ground-Based Magnetometer Initiative". In: *Eos, Transactions American Geophysical Union* 90.27, pp. 230–231. ISSN: 2324-9250. DOI: 10.1029/2009EO270002.

Gjerloev, J. W. (2012). "The SuperMAG Data Processing Technique". In: *Journal of Geophysical Research: Space Physics* 117.A9. ISSN: 2156-2202. DOI: 10.1029/2012JA017683.

Goncharov, O., H. Gunell, M. Hamrin and S. Chong (2020). "Evolution of High-Speed Jets and Plasmoids Downstream of the Quasi-Perpendicular Bow Shock". In: *Journal of Geophysical Research: Space Physics* 125.6, e2019JA027667. ISSN: 2169-9402. DOI: 10.1029/2019JA027667.

Graham, D. B. et al. (2017). "Lower Hybrid Waves in the Ion Diffusion and Magnetospheric Inflow Regions". In: *Journal of Geophys-*

ical Research: Space Physics 122.1, pp. 517–533. ISSN: 2169-9402. DOI: 10.1002/2016JA023572.

Greenwald, R. A. et al. (1995). "DARN/SuperDARN". In: *Space Science Reviews* 71.1, pp. 761–796. ISSN: 1572-9672. DOI: 10.1007/BF00751350.

Grimmich, Niklas, Ferdinand Plaschke, Martin O. Archer, Daniel Heyner, Johannes Z. D. Mieth, Rumi Nakamura and David G. Sibeck (2023). "Study of Extreme Magnetopause Distortions Under Varying Solar Wind Conditions". In: *Journal of Geophysical Research: Space Physics* 128.8, e2023JA031603. ISSN: 2169-9380, 2169-9402. DOI: 10.1029/2023JA031603.

Gunell, H., H. Nilsson, G. Stenberg, M. Hamrin, T. Karlsson, R. Maggiolo, M. André, R. Lundin and I. Dandouras (2012). "Plasma Penetration of the Dayside Magnetopause". In: *Physics of Plasmas* 19.7, p. 072906. ISSN: 1070-664X, 1089-7674. DOI: 10.1063/1.4739446.

Gunell, H. et al. (2014). "Waves in High-Speed Plasmoids in the Magnetosheath and at the Magnetopause". In: *Annales Geophysicae* 32.8, pp. 991–1009. ISSN: 1432-0576. DOI: 10.5194/angeo-32-991-2014.

Gunell, Herbert, Charlotte Goetz and Shahab Fatemi (2024). "Impact of Radial Interplanetary Magnetic Fields on the Inner Coma of Comet 67P/Churyumov-Gerasimenko - Hybrid Simulations of the Plasma Environment". In: *Astronomy & Astrophysics* 682, A62. ISSN: 0004-6361, 1432-0746. DOI: 10.1051/0004-6361/202348186.

Gunell, Herbert, Maria Hamrin, Sara Nesbit-Östman, Eva Krämer and Hans Nilsson (2023). "Magnetosheath Jets at Mars". In: *Science Advances* 9.22, eadg5703. ISSN: 2375-2548. DOI: 10.1126/sciadv.adg5703.

Guo, Jin et al. (2025). "Three-Dimensional Global Hybrid Simulation of Magnetosheath Jets at Mercury". In: *The Astrophysical Journal Letters* 978.1, p. L9. ISSN: 2041-8205, 2041-8213. DOI: 10.3847/2041-8213/ad9dd7.

Halekas, J. S., E. R. Taylor, G. Dalton, G. Johnson, D. W. Curtis, J. P. McFadden, D. L. Mitchell, R. P. Lin and B. M. Jakosky (2015). "The Solar Wind Ion Analyzer for MAVEN". In: *Space Science Reviews* 195.1, pp. 125–151. ISSN: 1572-9672. DOI: 10.1007/s11214-013-0029-z.

Harten, Ronald and Kenn Clark (1995). "The Design Features of the GGS Wind and Polar Spacecraft". In: *Space Science Reviews* 71.1, pp. 23–40. ISSN: 1572-9672. DOI: 10.1007/BF00751324.

Hartinger, M. D., D. L. Turner, F. Plaschke, V. Angelopoulos and H. Singer (2013). "The Role of Transient Ion Foreshock Phenomena in Driving Pc5 ULF Wave Activity". In: *Journal of Geophysical Research: Space Physics* 118.1, pp. 299–312. ISSN: 2169-9380, 2169-9402. DOI: 10.1029/2012JA018349.

Hietala, H, D Trotta, A Fedeli, L B Wilson, L Vuorinen and J T Coburn (2024). "Candidates for Downstream Jets at Interplanetary Shocks". In: *Monthly Notices of the Royal Astronomical Society* 531.2, pp. 2415–2421. ISSN: 0035-8711, 1365-2966. DOI: 10.1093/mnras/stae1294.

Hietala, H., T. V. Laitinen, K. Andréeová, R. Vainio, A. Vaivads, M. Palmroth, T. I. Pulkkinen, H. E.J. Koskinen, E. A. Lucek and H. Rème (2009). "Supermagnetosonic Jets behind a Collisionless Quasiparallel Shock". In: *Physical Review Letters* 103.24, pp. 20–23. ISSN: 00319007. DOI: 10.1103/PhysRevLett.103.245001.

Hietala, H., N. Partamies, T. V. Laitinen, L. B. N. Clausen, G. Facskó, A. Vaivads, H. E. J. Koskinen, I. Dandouras, H. Rème and E. A. Lucek (2012). "Supermagnetosonic Subsolar Magnetosheath Jets and Their Effects: From the Solar Wind to the Ionospheric Convection". In: *Annales Geophysicae* 30.1, pp. 33–48. ISSN: 0992-7689. DOI: 10.5194/angeo-30-33-2012.

Hietala, H., T. D. Phan, V. Angelopoulos, M. Oieroset, M. O. Archer, T. Karlsson and F. Plaschke (2018). "In Situ Observations of a Magnetosheath High-Speed Jet Triggering Magnetopause Reconnection". In: *Geophysical Research Letters* 45.4, pp. 1732–1740. ISSN: 0094-8276, 1944-8007. DOI: 10.1002/2017GL076525.

Hietala, H. and F. Plaschke (2013). "On the Generation of Magnetosheath High-Speed Jets by Bow Shock Ripples". In: *Journal of Geophysical Research: Space Physics* 118.11, pp. 7237–7245. ISSN: 21699402. DOI: 10.1002/2013JA019172.

Hoppe, M. M., C. T. Russell, L. A. Frank, T. E. Eastman and E. W. Greenstadt (1981). "Upstream Hydromagnetic Waves and Their Association with Backstreaming Ion Populations: ISEE 1 and 2 Observations". In: *Journal of Geophysical Research: Space Physics* 86.A6, pp. 4471–4492. ISSN: 2156-2202. DOI: 10.1029/JA086iA06p04471.

Jacobsen, K. S. et al. (2009). "THEMIS Observations of Extreme Magnetopause Motion Caused by a Hot Flow Anomaly". In: *Journal of Geophysical Research: Space Physics* 114.A8. ISSN: 2156-2202. DOI: 10.1029/2008JA013873.

Jakosky, B. M. et al. (2015). "The Mars Atmosphere and Volatile Evolution (MAVEN) Mission". In: *Space Science Reviews* 195.1, pp. 3–48. ISSN: 1572-9672. DOI: 10.1007/s11214-015-0139-x.

Jiang, Wence, Daniel Verscharen, Seong-Yeop Jeong, Hui Li, Kristopher G. Klein, Christopher J. Owen and Chi Wang (2024). "Velocity-Space Signatures of Resonant Energy Transfer between Whistler Waves and Electrons in the Earth's Magnetosheath". In: *The Astrophysical Journal* 960.1, p. 30. ISSN: 0004-637X, 1538-4357. DOI: 10.3847/1538-4357/ad0df8.

Johlander, A. et al. (2016). "Rippled Quasiperpendicular Shock Observed by the Magnetospheric Multiscale Spacecraft". In: *Physical Review Letters* 117.16, p. 165101. DOI: 10.1103/PhysRevLett.117.165101.

Johnson, Jay R., Simon Wing and Peter A. Delamere (2014). "Kelvin Helmholtz Instability in Planetary Magnetospheres". In: *Space Science Reviews* 184.1, pp. 1–31. ISSN: 1572-9672. DOI: 10.1007/s11214-014-0085-z.

Kajdič, Primož, Savvas Raptis, Xóchitl Blanco-Cano and Tomas Karlsson (2021). "Causes of Jets in the Quasi-Perpendicular Magnetosheath". In: *Geophysical Research Letters* 48.13, e2021GL093173. ISSN: 1944-8007. DOI: 10.1029/2021GL093173.

Kajdič, Primož et al. (2024). "Transient Upstream Mesoscale Structures: Drivers of Solar-Quiet Space Weather". In: *Frontiers in Astronomy and Space Sciences* 11. ISSN: 2296-987X. DOI: 10.3389/fspas.2024.1436916.

Karimabadi, H. et al. (2014). "The Link between Shocks, Turbulence, and Magnetic Reconnection in Collisionless Plasmas". In: *Physics of Plasmas* 21.6, p. 062308. ISSN: 1070-664X. DOI: 10.1063/1.4882875.

Karlsson, T., N. Brenning, H. Nilsson, J. G. Trotignon, X. Valliéres and G. Facsko (2012). "Localized Density Enhancements in the Magnetosheath: Three-dimensional Morphology and Possible Importance for Impulsive Penetration". In: *Journal of Geophysical Research: Space Physics* 117.3, pp. 1–14. ISSN: 21699402. DOI: 10.1029/2011JA017059.

Karlsson, T., A. Kullen, E. Liljeblad, N. Brenning, H. Nilsson, H. Gunell and M. Hamrin (2015). "On the Origin of Magnetosheath Plasmoids and Their Relation to Magnetosheath Jets". In: *Journal of Geophysical Research: Space Physics* 120.9, pp. 7390–7403. ISSN: 2169-9380, 2169-9402. DOI: 10.1002/2015JA021487.

Karlsson, Tomas, Ferdinand Plaschke, Heli Hietala, Martin Archer, Xóchitl Blanco-Cano, Primož Kajdič, Per Arne Lindqvist, Göran Marklund and Daniel J. Gershman (2018). "Investigating the Anatomy of Magnetosheath Jets - MMS Observations". In: *Annales Geophysicae* 36.2, pp. 655–677. ISSN: 14320576. DOI: 10.5194/angeo-36-655-2018.

Kim, Hyangpyo, Rumi Nakamura, Niklas Grimmich, Adriana Settino, Kyoung-Joo Hwang, Jaeheung Park, Zoltán Vörös, Cyril Simon Wedlund and Kathryn A. McWilliams (2025). "Extreme Magnetopause Deformation Induced by High-Speed Jet From Foreshock Transient". In: *Geophysical Research Letters* 52.20, e2025GL117683. ISSN: 1944-8007. DOI: 10.1029/2025GL117683.

Koskinen, Hannu EJ and Emilia KJ Kilpua (2022). *Physics of Earth's radiation belts: Theory and observations*. Springer Nature.

Krämer, E., M. Hamrin, H. Gunell, L. Baddeley, N. Partamies, S. Raptis, K. Herlingshaw and A. Schillings (2025). "Magnetosheath Jet-Triggered ULF Waves: Energy Deposition in the Ionosphere". In: *Journal of Geophysical Research: Space Physics* 130.4, e2025JA033792. ISSN: 2169-9380, 2169-9402. DOI: 10.1029/2025JA033792.

Krämer, E., M. Hamrin, H. Gunell, T. Karlsson, K. Steinvall, O. Goncharov and Mats André (2023). "Waves in Magnetosheath Jets—Classification and the Search for Generation Mechanisms Using MMS Burst Mode Data". In: *Journal of Geophysical Research: Space Physics* 128.7, e2023JA031621. ISSN: 2169-9380, 2169-9402. DOI: 10.1029/2023JA031621.

Krämer, Eva, Shahab Fatemi, Maria Hamrin, Herbert Gunell and Gabriella Nordin (2025). "On the Kinetic Energy Input of Magnetosheath

Jets Into the Magnetosheath". In: *Geophysical Research Letters* 52.15, e2025GL115260. ISSN: 1944-8007. DOI: 10.1029/2025GL115260.

Krämer, Eva et al. (2024). "Jets Downstream of Collisionless Shocks: Recent Discoveries and Challenges". In: *Space Science Reviews* 221.1, p. 4. ISSN: 1572-9672. DOI: 10.1007/s11214-024-01129-3.

Lapenta, Giovanni (2016). "Particle in cell methods". In: *With Application to Simulations in Space. Weather*. Citeseer.

Le Contel, O. et al. (2016). "The Search-Coil Magnetometer for MMS". In: *Space Science Reviews* 199.1, pp. 257–282. ISSN: 1572-9672. DOI: 10.1007/s11214-014-0096-9.

Ledvina, SA, Y-J Ma and E Kallio (2008). "Modeling and simulating flowing plasmas and related phenomena". In: *Space Science Reviews* 139.1, pp. 143–189.

Lindqvist, P.-A. et al. (2016). "The Spin-Plane Double Probe Electric Field Instrument for MMS". In: *Space Science Reviews* 199.1, pp. 137–165. ISSN: 1572-9672. DOI: 10.1007/s11214-014-0116-9.

Liu, Terry Z., Heli Hietala, Vassilis Angelopoulos, Yuri Omelchenko, Vadim Roytershteyn and Rami Vainio (2019). "THEMIS Observations of Particle Acceleration by a Magnetosheath Jet-Driven Bow Wave". In: *Geophysical Research Letters* 46.14, pp. 7929–7936. ISSN: 0094-8276, 1944-8007. DOI: 10.1029/2019GL082614.

Lucek, E. A., T. S. Horbury, M. W. Dunlop, P. J. Cargill, S. J. Schwartz, A. Balogh, P. Brown, C. Carr, K.-H. Fornacon and E. Georgescu (2002). "Cluster Magnetic Field Observations at a Quasi-Parallel Bow Shock". In: *Annales Geophysicae* 20.11, pp. 1699–1710. ISSN: 0992-7689. DOI: 10.5194/angeo-20-1699-2002.

Lucek, EA, D Constantinescu, ML Goldstein, J Pickett, Jean-Louis Pincon, F Sahraoui, RA Treumann and SN Walker (2005). "The magnetosheath". In: *Space Science Reviews* 118.1, pp. 95–152. DOI: 10.1007/s11214-005-3825-2.

Ma, Xuanye, Katariina Nykyri, Andrew Dimmock and Christina Chu (2020). "Statistical study of solar wind, magnetosheath, and magnetotail plasma and field properties: 12+ years of THEMIS observations and MHD simulations". In: *Journal of Geophysical Research: Space Physics* 125.10, e2020JA028209.

Mailyan, B, C Munteanu and S Haaland (2008). "What is the best method to calculate the solar wind propagation delay?" In: *Annales geophysicae*. Vol. 26. 8. Copernicus GmbH, pp. 2383–2394.

Mathie, R. A. and I. R. Mann (2000). "A Correlation between Extended Intervals of Ulf Wave Power and Storm-Time Geosynchronous Relativistic Electron Flux Enhancements". In: *Geophysical Research Letters* 27.20, pp. 3261–3264. ISSN: 1944-8007. DOI: 10.1029/2000GL003822.

Matsunaga, Kazunari et al. (2017). "Statistical Study of Relations Between the Induced Magnetosphere, Ion Composition, and Pressure Balance Boundaries Around Mars Based On MAVEN Observations".

In: *Journal of Geophysical Research: Space Physics* 122.9, pp. 9723–9737. ISSN: 2169-9402. DOI: 10.1002/2017JA024217.

Mauk, B. H., N. J. Fox, S. G. Kanekal, R. L. Kessel, D. G. Sibeck and A. Ukhorskiy (2013). "Science Objectives and Rationale for the Radiation Belt Storm Probes Mission". In: *Space Science Reviews* 179.1–4, pp. 3–27. ISSN: 0038-6308, 1572-9672. DOI: 10.1007/s11214-012-9908-y.

Maxwell, James Clerk (1865). "VIII. A dynamical theory of the electromagnetic field". In: *Philosophical transactions of the Royal Society of London* 155, pp. 459–512.

McFadden, J. P., C. W. Carlson, D. Larson, M. Ludlam, R. Abiad, B. Elliott, P. Turin, M. Marckwordt and V. Angelopoulos (2008). "The THEMIS ESA Plasma Instrument and In-flight Calibration". In: *Space Science Reviews* 141.1, pp. 277–302. ISSN: 1572-9672. DOI: 10.1007/s11214-008-9440-2.

Menk, Frederick W. (2011). "Magnetospheric ULF Waves: A Review". In: *The Dynamic Magnetosphere*. Ed. by William Liu and Masaki Fujimoto. Dordrecht: Springer Netherlands, pp. 223–256. ISBN: 978-94-007-0500-5 978-94-007-0501-2. DOI: 10.1007/978-94-007-0501-2_13.

Miura, Akira and P. L. Pritchett (1982). "Nonlocal Stability Analysis of the MHD Kelvin-Helmholtz Instability in a Compressible Plasma". In: *Journal of Geophysical Research: Space Physics* 87.A9, pp. 7431–7444. ISSN: 2156-2202. DOI: 10.1029/JA087iA09p07431.

Miyoshi, Yoshizumi et al. (2018). "Geospace Exploration Project ERG". In: *Earth, Planets and Space* 70.1, p. 101. ISSN: 1880-5981. DOI: 10.1186/s40623-018-0862-0.

Moeslinger, A., H. Gunell, H. Nilsson, S. Fatemi and G. Stenberg Wieser (2024). "Explaining the Evolution of Ion Velocity Distributions at a Low Activity Comet". In: *Journal of Geophysical Research: Space Physics* 129.9, e2024JA032757. ISSN: 2169-9402. DOI: 10.1029/2024JA032757.

Moeslinger, Anja, Herbert Gunell, Gabriella Stenberg Wieser, Hans Nilsson and Shahab Fatemi (2025). "Kinetic-Scale Physics of Multi-Species Solar Wind - Interaction with a Comet". In: *Astronomy & Astrophysics* 703, A173. ISSN: 0004-6361, 1432-0746. DOI: 10.1051/0004-6361/202452636.

Mohammed-Amin, Tara, Eva Krämer, Sara Nesbit-Östman, Herbert Gunell and Cyril Simon Wedlund (2025). "Jets Downstream of the Martian Bow Shock: Occurrence in the 2014–2024 Period". In: *Astronomy & Astrophysics* 696, A75. ISSN: 0004-6361, 1432-0746. DOI: 10.1051/0004-6361/202453557.

Murphy, Kyle R., Ian R. Mann, I. Jonathan Rae and David K. Milling (2011). "Dependence of Ground-Based Pc5 ULF Wave Power on F10.7 Solar Radio Flux and Solar Cycle Phase". In: *Journal of Atmospheric and Solar-Terrestrial Physics*. Influence of Solar Activity on Interplanetary and Geophysical Phenomena 73.11, pp. 1500–1510. ISSN: 1364-6826. DOI: 10.1016/j.jastp.2011.02.018.

Němeček, Z., J. Šafránková, K. Grygorov, A. Mokrý, G. Pi, M. Aghabozorgi Nafchi, F. Němec, N. Xirogiannopoulou and J. Šimůnek (2023). "Extremely Distant Magnetopause Locations Caused by Magnetosheath Jets". In: *Geophysical Research Letters* 50.24, e2023GL106131. ISSN: 0094-8276, 1944-8007. DOI: 10.1029/2023GL106131.

Nesbit-Östman, Sara (2025). "Structure of the Martian Bow Shock". In.

Norenius, L., M. Hamrin, O. Goncharov, H. Gunell, H. Opgenoorth, T. Pitkänen, S. Chong, N. Partamies and L. Baddeley (2021). "Ground-Based Magnetometer Response to Impacting Magnetosheath Jets". In: *Journal of Geophysical Research: Space Physics* 126.8. ISSN: 2169-9380, 2169-9402. DOI: 10.1029/2021JA029115.

Norgren, Cecilia, Andris Vaivads, Yuri V. Khotyaintsev and Mats André (2012). "Lower Hybrid Drift Waves: Space Observations". In: *Physical Review Letters* 109.5, p. 055001. ISSN: 0031-9007, 1079-7114. DOI: 10.1103/PhysRevLett.109.055001.

Omelchenko, Y. A., L.-J. Chen and J. Ng (2021). "3D Space-Time Adaptive Hybrid Simulations of Magnetosheath High-Speed Jets". In: *Journal of Geophysical Research: Space Physics* 126.7, e2020JA029035. ISSN: 2169-9402. DOI: 10.1029/2020JA029035.

Palmroth, Minna et al. (2018). "Magnetosheath Jet Properties and Evolution as Determined by a Global Hybrid-Vlasov Simulation". In: *Annales Geophysicae* 36.5, pp. 1171–1182. ISSN: 0992-7689. DOI: 10.5194/angeo-36-1171-2018.

Palmroth, Minna et al. (2020). "Magnetosheath Jet Evolution as a Function of Lifetime: Global Hybrid-Vlasov Simulations Compared to MMS Observations". In: *Annales Geophysicae* 39.2, pp. 289–308. DOI: 10.5194/angeo-2020-49.

Papitashvili, Natalia E. and Joseph H. King (2020). *OMNI 1-min Data [Data set]*. DOI: https://doi.org/10.48322/45bb-8792.

Parker, Eugene N (1958). "Dynamics of the interplanetary gas and magnetic fields." In: *Astrophysical Journal, vol. 128, p. 664* 128, p. 664. DOI: 10.1086/146579.

Picone, J. M., A. E. Hedin, D. P. Drob and A. C. Aikin (2002). "NRLMSISE-00 empirical model of the atmosphere: Statistical comparisons and scientific issues". In: *Journal of Geophysical Research: Space Physics* 107.A12, SIA 15-1-SIA 15–16. DOI: https://doi.org/10.1029/2002JA009430. eprint: https://agupubs.onlinelibrary.wiley.com/doi/pdf/10.1029/2002JA009430.

Plaschke, F., H. Hietala and V. Angelopoulos (2013). "Anti-Sunward High-Speed Jets in the Subsolar Magnetosheath". In: *Annales Geophysicae* 31.10, pp. 1877–1889. ISSN: 09927689. DOI: 10.5194/angeo-31-1877-2013.

Plaschke, Ferdinand and Heli Hietala (2018). "Plasma Flow Patterns in and around Magnetosheath Jets". In: *Annales Geophysicae* 36.3, pp. 695–703. ISSN: 1432-0576. DOI: 10.5194/angeo-36-695-2018.

Plaschke, Ferdinand, Heli Hietala, Vassilis Angelopoulos and Rumi Nakamura (2016). "Geoeffective Jets Impacting the Magnetopause Are Very Common." In: *Journal of Geophysical Research* 121.4, pp. 3240–3253. DOI: 10.1002/2016ja022534. PMID: 27478719.

Plaschke, Ferdinand, Heli Hietala and Zoltan Vörös (2020). "Scale Sizes of Magnetosheath Jets". In: *Journal of Geophysical Research: Space Physics* 125.9. ISSN: 2169-9380, 2169-9402. DOI: 10.1029/2020JA027962.

Plaschke, Ferdinand, Heli Hietala et al. (2018). "Jets Downstream of Collisionless Shocks". In: *Space Science Reviews* 214.5, p. 81. ISSN: 0038-6308, 1572-9672. DOI: 10.1007/s11214-018-0516-3.

Plaschke, Ferdinand, Maria Jernej, Heli Hietala and Laura Vuorinen (2020). "On the Alignment of Velocity and Magnetic Fields within Magnetosheath Jets". In: *Annales Geophysicae* 38.2, pp. 287–296. ISSN: 14320576. DOI: 10.5194/angeo-38-287-2020.

Pollock, C. et al. (2016). "Fast Plasma Investigation for Magnetospheric Multiscale". In: *Space Science Reviews* 199.1, pp. 331–406. ISSN: 1572-9672. DOI: 10.1007/s11214-016-0245-4.

Qiu, Hui-Xuan, De-Sheng Han, Run Shi and Jianjun Liu (2024). "Magnetosheath High-Speed Jet Drives Multiple Auroral Arcs Near Local Noon". In: *AGU Advances* 5.5, e2024AV001197. ISSN: 2576-604X. DOI: 10.1029/2024AV001197.

Rae, I. J., C. E. J. Watt, F. R. Fenrich, I. R. Mann, L. G. Ozeke and A. Kale (2007). "Energy Deposition in the Ionosphere through a Global Field Line Resonance". In: *Annales Geophysicae* 25.12, pp. 2529–2539. ISSN: 1432-0576. DOI: 10.5194/angeo-25-2529-2007.

Raptis, Savvas, Tomas Karlsson, Ferdinand Plaschke, Anita Kullen and Per-Arne Lindqvist (2020). "Classifying Magnetosheath Jets Using MMS: Statistical Properties". In: *Journal of Geophysical Research: Space Physics* 125.11, e2019JA027754. ISSN: 2169-9380, 2169-9402. DOI: 10.1029/2019JA027754.

Raptis, Savvas, Tomas Karlsson, Andris Vaivads, Martin Lindberg, Andreas Johlander and Henriette Trollvik (2022). "On Magnetosheath Jet Kinetic Structure and Plasma Properties". In: *Geophysical Research Letters* 49.21, e2022GL100678. ISSN: 1944-8007. DOI: 10.1029/2022GL100678.

Raptis, Savvas, Tomas Karlsson, Andris Vaivads, Craig Pollock, Ferdinand Plaschke, Andreas Johlander, Henriette Trollvik and Per-Arne Lindqvist (2022). "Downstream High-Speed Plasma Jet Generation as a Direct Consequence of Shock Reformation". In: *Nature Communications* 13.1, p. 598. ISSN: 2041-1723. DOI: 10.1038/s41467-022-28110-4.

Raptis, Savvas et al. (2025). "Multimission Observations of Relativistic Electrons and High-speed Jets Linked to Shock-generated Transients". In: *The Astrophysical Journal Letters* 981.1, p. L10. ISSN: 2041-8205. DOI: 10.3847/2041-8213/adb154.

Redhead, PA (1999). *Extreme high vacuum*. Tech. rep. Cern.

Ren, Junyi, Jin Guo, Quanming Lu, San Lu, Xinliang Gao, Jiuqi Ma and Rongsheng Wang (2024). "Honeycomb-Like Magnetosheath Structure Formed by Jets: Three-Dimensional Global Hybrid Simulations". In: *Geophysical Research Letters* 51.12, e2024GL109925. ISSN: 0094-8276, 1944-8007. DOI: 10.1029/2024GL109925.

Retinò, Alessandro, Yuri Khotyaintsev, Olivier Le Contel, Maria Federica Marcucci, Ferdinand Plaschke, Andris Vaivads, Vassilis Angelopoulos, Pasquale Blasi, Jim Burch, Johan De Keyser et al. (2022). "Particle energization in space plasmas: towards a multi-point, multiscale plasma observatory". In: *Experimental Astronomy* 54.2, pp. 427–471.

Roberts, O. W., Z. Vörös, A. Settino, F. Koller, S. Raptis, M. Temmer, C. Simon Wedlund, X. Li and R. Nakamura (2025). "Energy Conversion and Exchange in a Magnetosheath Jet". In: *Journal of Geophysical Research: Space Physics* 130.11, e2025JA034414. ISSN: 2169-9402. DOI: 10.1029/2025JA034414.

Russell, C. T., B. J. Anderson et al. (2016). "The Magnetospheric Multiscale Magnetometers". In: *Space Science Reviews* 199.1, pp. 189–256. ISSN: 1572-9672. DOI: 10.1007/s11214-014-0057-3.

Russell, Christopher T, Janet G Luhmann and Robert J Strangeway (2016). *Space physics: An introduction*. Cambridge University Press.

Savin, S. et al. (2012). "Super Fast Plasma Streams as Drivers of Transient and Anomalous Magnetospheric Dynamics". In: *Annales Geophysicae* 30.1, pp. 1–7. ISSN: 1432-0576. DOI: 10.5194/angeo-30-1-2012.

Schwartz, Steven J. and David Burgess (1991). "Quasi-Parallel Shocks: A Patchwork of Three-Dimensional Structures". In: *Geophysical Research Letters* 18.3, pp. 373–376. ISSN: 1944-8007. DOI: 10.1029/91GL00138.

Schwartz, Steven J., David Burgess, William P. Wilkinson, Ramona L. Kessel, Malcolm Dunlop and Hermann Lühr (1992). "Observations of Short Large-Amplitude Magnetic Structures at a Quasi-Parallel Shock". In: *Journal of Geophysical Research: Space Physics* 97.A4, pp. 4209–4227. ISSN: 2156-2202. DOI: 10.1029/91JA02581.

Shan, Lican, Quanming Lu, Christian Mazelle, Can Huang, Tielong Zhang, Mingyu Wu, Xinliang Gao and Shui Wang (2015). "The Shape of the Venusian Bow Shock at Solar Minimum and Maximum: Revisit Based on VEX Observations". In: *Planetary and Space Science* 109–110, pp. 32–37. ISSN: 00320633. DOI: 10.1016/j.pss.2015.01.004.

Shi, Z. et al. (2025). "Mercury's Field-Aligned Currents: Perspectives From Hybrid Simulations". In: *Journal of Geophysical Research: Planets* 130.2, e2024JE008610. ISSN: 2169-9100. DOI: 10.1029/2024JE008610.

Shue, J.-H. et al. (1998). "Magnetopause Location under Extreme Solar Wind Conditions". In: *Journal of Geophysical Research: Space Physics* 103.A8, pp. 17691–17700. ISSN: 2156-2202. DOI: 10.1029/98JA01103.

Shue, J.-H., J. K. Chao, H. C. Fu, C. T. Russell, P. Song, K. K. Khurana and H. J. Singer (1997). "A New Functional Form to Study the Solar Wind Control of the Magnetopause Size and Shape". In: *Journal of Geophysical Research: Space Physics* 102.A5, pp. 9497–9511. ISSN: 0148-0227. DOI: 10.1029/97JA00196.

Shue, J.-H. and J.-K. Chao (2013). "The Role of Enhanced Thermal Pressure in the Earthward Motion of the Earth's Magnetopause". In: *Journal of Geophysical Research: Space Physics* 118.6, pp. 3017–3026. ISSN: 2169-9380, 2169-9402. DOI: 10.1002/jgra.50290.

Shue, Jih-Hong et al. (2009). "Anomalous Magnetosheath Flows and Distorted Subsolar Magnetopause for Radial Interplanetary Magnetic Fields". In: *Geophysical Research Letters* 36.18. DOI: 10.1029/2009gl039842.

Stone, E C, A M Frandsen, R A Mewaldt, E R Christian, D Margolies, J F Ormes and F Snow (1998). "The Advanced Composition Explorer". In: *Space Science Reviews* 86.1, pp. 1–22.

Suni, J. et al. (2021). "Connection Between Foreshock Structures and the Generation of Magnetosheath Jets: Vlasiator Results". In: *Geophysical Research Letters* 48.20. ISSN: 0094-8276, 1944-8007. DOI: 10.1029/2021GL095655.

Suni, Jonas, Minna Palmroth, Lucile Turc, Markus Battarbee, Yann Pfau-Kempf and Urs Ganse (2025). "Magnetosheath Jets Associated With a Solar Wind Rotational Discontinuity in a Hybrid-Vlasov Simulation". In: *Journal of Geophysical Research: Space Physics* 130.6, e2025JA033995. ISSN: 2169-9402. DOI: 10.1029/2025JA033995.

Svalgaard, Leif and John M. Wilcox (1974). "The Spiral Interplanetary Magnetic Field: A Polarity and Sunspot Cycle Variation". In: *Science* 186.4158, pp. 51–53. ISSN: 0036-8075, 1095-9203. DOI: 10.1126/science.186.4158.51.

Thomsen, MF, SJ Schwartz and JT Gosling (1983). "Observational evidence on the origin of ions upstream of the Earth's bow shock". In: *Journal of Geophysical Research: Space Physics* 88.A10, pp. 7843–7852. DOI: 10.1029/JA088iA10p07843.

Torbert, R. B. et al. (2016). "The FIELDS Instrument Suite on MMS: Scientific Objectives, Measurements, and Data Products". In: *Space Science Reviews* 199.1, pp. 105–135. ISSN: 1572-9672. DOI: 10.1007/s11214-014-0109-8.

Torkar, K., R. Nakamura, M. Tajmar, C. Scharlemann, H. Jeszenszky, G. Laky, G. Fremuth, C. P. Escoubet and K. Svenes (2016). "Active Spacecraft Potential Control Investigation". In: *Space Science Reviews* 199.1, pp. 515–544. ISSN: 1572-9672. DOI: 10.1007/s11214-014-0049-3.

Tóth, Gábor, Yuxi Chen, Tamas I. Gombosi, Paul Cassak, Stefano Markidis and Ivy Bo Peng (2017). "Scaling the Ion Inertial Length and Its Implications for Modeling Reconnection in Global Simulations". In:

Journal of Geophysical Research: Space Physics 122.10. ISSN: 2169-9380, 2169-9402. DOI: 10.1002/2017JA024189.

Tsyganenko, N. A. (1989). "A Magnetospheric Magnetic Field Model with a Warped Tail Current Sheet". In: *Planetary and Space Science* 37.1, pp. 5–20. ISSN: 0032-0633. DOI: 10.1016/0032-0633(89)90066-4.

Tsyganenko, N. A. (1995). "Modeling the Earth's Magnetospheric Magnetic Field Confined within a Realistic Magnetopause". In: *Journal of Geophysical Research: Space Physics* 100.A4, pp. 5599–5612. ISSN: 2156-2202. DOI: 10.1029/94JA03193.

Tsyganenko, N. A. and M. I. Sitnov (2005). "Modeling the Dynamics of the Inner Magnetosphere during Strong Geomagnetic Storms". In: *Journal of Geophysical Research: Space Physics* 110.A3. ISSN: 2156-2202. DOI: 10.1029/2004JA010798.

Tsyganenko, No A (1996). "Effects of the solar wind conditions in the global magnetospheric configurations as deduced from data-based field models". In: *International conference on substorms*. Vol. 389, p. 181.

Turc, Lucile, Vertti Tarvus, Andrew P. Dimmock, Markus Battarbee, Urs Ganse, Andreas Johlander, Maxime Grandin, Yann Pfau-Kempf, Maxime Dubart and Minna Palmroth (2020). "Asymmetries in the Earth's Dayside Magnetosheath: Results from Global Hybrid-Vlasov Simulations". In: *Annales Geophysicae* 38.5, pp. 1045–1062. ISSN: 0992-7689. DOI: 10.5194/angeo-38-1045-2020.

Von Alfthan, S, D Pokhotelov, Y Kempf, S Hoilijoki, I Honkonen, A Sandroos and M Palmroth (2014). "Vlasiator: First global hybrid-Vlasov simulations of Earth's foreshock and magnetosheath". In: *Journal of Atmospheric and Solar-Terrestrial Physics* 120, pp. 24–35.

Vuorinen, Laura, Heli Hietala, Adrian T. LaMoury and Ferdinand Plaschke (2023). "Solar Wind Parameters Influencing Magnetosheath Jet Formation: Low and High IMF Cone Angle Regimes". In: *Journal of Geophysical Research: Space Physics* 128.10, e2023JA031494. ISSN: 2169-9402. DOI: 10.1029/2023JA031494.

Vuorinen, Laura, Heli Hietala and Ferdinand Plaschke (2019). "Jets in the Magnetosheath: IMF Control of Where They Occur". In: *Annales Geophysicae* 37.4, pp. 689–697. ISSN: 0992-7689. DOI: 10.5194/angeo-37-689-2019.

Walt, Martin (1994). "Introduction to geomagnetically trapped radiation." In: *Camb. Atmos. Space Sci. Ser* 10.

Wang, Boyi, Yukitoshi Nishimura, Heli Hietala and Vassilis Angelopoulos (2022). "Investigating the Role of Magnetosheath High-Speed Jets in Triggering Dayside Ground Magnetic Ultra-Low Frequency Waves". In: *Geophysical Research Letters* 49.22, e2022GL099768. ISSN: 0094-8276, 1944-8007. DOI: 10.1029/2022GL099768.

Wang, Boyi, Yukitoshi Nishimura, Heli Hietala, Larry Lyons, Vassilis Angelopoulos, Ferdinand Plaschke, Yusuke Ebihara and Allan Weatherwax (2018). "Impacts of Magnetosheath High-Speed Jets on the

Magnetosphere and Ionosphere Measured by Optical Imaging and Satellite Observations". In: *Journal of Geophysical Research: Space Physics* 123.6, pp. 4879–4894. ISSN: 2169-9402. DOI: 10.1029/2017JA024954.

Wang, Chi, XiaoCheng Guo, Zhong Peng, BinBin Tang, TianRan Sun, WenYa Li and YouQiu Hu (2013). "Magnetohydrodynamics (MHD) numerical simulations on the interaction of the solar wind with the magnetosphere: A review". In: *Science China Earth Sciences* 56.7, pp. 1141–1157.

Wang, Xiao-Dong, Shahab Fatemi, Mats Holmström, Hans Nilsson, Yoshifumi Futaana and Stas Barabash (2024). "Martian Global Current Systems and Related Solar Wind Energy Transfer: Hybrid Simulation under Nominal Conditions". In: *Monthly Notices of the Royal Astronomical Society* 527.4, pp. 12232–12242. ISSN: 0035-8711. DOI: 10.1093/mnras/stad3486.

Wannberg, G. et al. (1997). "The EISCAT Svalbard Radar: A Case Study in Modern Incoherent Scatter Radar System Design". In: *Radio Science* 32.6, pp. 2283–2307. ISSN: 1944-799X. DOI: 10.1029/97RS01803.

Wilson, L. B. (2016). *Low Frequency Waves at and Upstream of Collisionless Shocks*. AGU Journals. URL: https://onlinelibrary.wiley.com/doi/abs/10.1002/9781119055006.ch16 (visited on 27/04/2026).

Xirogiannopoulou, N., O. Goncharov, J. Šafránková and Z. Němeček (2026). "Relationship Between Foreshock Structures and Magnetosheath Jets". In: *Journal of Geophysical Research: Space Physics* 131.4, e2026JA035161. ISSN: 2169-9402. DOI: 10.1029/2026JA035161.

Xu, Shaosui, Michael W. Liemohn, Chuanfei Dong, David L. Mitchell, Stephen W. Bougher and Yingjuan Ma (2016). "Pressure and Ion Composition Boundaries at Mars". In: *Journal of Geophysical Research: Space Physics* 121.7, pp. 6417–6429. ISSN: 2169-9402. DOI: 10.1002/2016JA022644.

Zhang, Chi et al. (2025). "Role of ULF Waves in Reforming the Martian Bow Shock". In: *AGU Advances* 6.4, e2025AV001654. ISSN: 2576-604X, 2576-604X. DOI: 10.1029/2025AV001654.

Zhang, Hui, Qiugang Zong, Hyunju Connor, Peter Delamere, Gábor Facskó, Desheng Han, Hiroshi Hasegawa, Esa Kallio, Árpád Kis, Guan Le et al. (2022). "Dayside transient phenomena and their impact on the magnetosphere and ionosphere". In: *Space Science Reviews* 218.5, p. 40. DOI: 10.1007/s11214-021-00865-0.

Zhang, Qi, Stas Barabash, Mats Holmstrom, Xiao-dong Wang, Yoshifumi Futaana, Christopher M. Fowler, Robin Ramstad and Hans Nilsson (2024). "Mars's Induced Magnetosphere Can Degenerate". In: *Nature* 634.8032, pp. 45–47. ISSN: 1476-4687. DOI: 10.1038/s41586-024-07959-z.

Zhou, Yufei, Savvas Raptis, Shan Wang, Chao Shen, Nian Ren and Lan Ma (2024). "Magnetosheath Jets at Jupiter and across the Solar System". In: *Nature Communications* 15.1, p. 4. ISSN: 2041-1723. DOI: 10.1038/s41467-023-43942-4.